Supplementary Materials for

Mapping the human DC lineage through the integration of high-dimensional techniques

Peter See,* Charles-Antoine Dutertre,* Jinmiao Chen,* Patrick Günther, Naomi McGovern, Sergio Erdal Irac, Merry Gunawan, Marc Beyer, Kristian Händler, Kaibo Duan, Hermi Rizal Bin Sumatoh, Nicolas Ruffin, Mabel Jouve, Ester Gea-Mallorquí, Raoul C. M. Hennekam, Tony Lim, Chan Chung Yip, Ming Wen, Benoit Malleret, Ivy Low, Nurhidaya Binte Shadan, Charlene Foong Shu Fen, Alicia Tay, Josephine Lum, Francesca Zolezzi, Anis Larbi, Michael Poidinger, Jerry K. Y. Chan, Qingfeng Chen, Laurent Renia, Muzlifah Haniffa, Philippe Benaroch, Andreas Schlitzer, Joachim L. Schultze, Evan W. Newell, Florent Ginhoux†

*These authors contributed equally to this work.
†Corresponding author. Email: florent_ginhoux@immunol.a-star.edu.sg

Published 4 May 2017 on *Science* First Release
DOI: 10.1126/science.aag3009

This PDF file includes:

Other Supplementary Material for this manuscript includes the following:
(available at www.sciencemag.org/cgi/content/full/science.aag3009/DC1)

Supplementary Materials and Methods

Validation of down sampling threshold for normalization of MARS-seq single cell transcriptome data

High variance in terms of quality of single-cell transcriptomes is expected in a single-cell RNA sequencing experiment due to the low quantity of RNA input material. This caveat necessitates stringent quality control in order to avoid a bias introduced by low quality single-cell transcriptomes. In single-cell transcriptomics it is, therefore, common practice to remove low quality transcriptomes to ensure an unbiased and biologically meaningful analysis (*71*, *72*). Different strategies have been used to filter out low quality cells, including an empirically determined cutoff for cell filtering (*71*), a down sampling strategy to normalize and filter low quality cells (*15*), and various filtering cutoffs from 600 UMIs/cell or 400 UMIs/cells (*15*), <500 molecule counts per cell (*73*) and<200 UMIs/cell (*74*). To the best of our knowledge, a mathematically determined cut-off was not reported in any of these studies. As these previous studies were performed on murine cells, and quality filters in single-cell data have to be established within the respective dataset, we had to adapt the filtering strategy to human cells. To determine the quality threshold for our dataset, several diagnostics were used to estimate the optimal cutoff for down sampling of molecule counts. Firstly, we visualized the cumulative distribution of molecule counts, where cells on the x-axis were ordered by decreasing UMI count (**fig. S1c**). Here, we noted that in a certain region there was a period of strong decline in the number of molecule counts per cell. This region corresponded to a range of molecule counts between 400 and 1200 UMIs per cell. The next metric used to judge an objective threshold (**fig. S1d**) was the molecule count distribution of all cells. We found that many of the cell barcodes had <650 molecule counts: these cell barcodes most likely represented the background signal of our MARS-seq data set. The number of cell barcodes with a certain number of molecules decreases with increasing molecule count per cell; through this visualization, we identified natural breakpoints in the distribution that could be used as an objective threshold for filtering and normalization, as these breakpoints mark a change in the data structure and quality, and indicate the transition from background to signal, or from low-quality transcriptomes to high-quality transcriptomes. Here, three notable points were identified (**fig. S1d**), which corresponded to molecule counts of 650 (blue), 1,050 (red) and 1,700 (green) per cell. To objectively determine which of these points represented a shift in data quality from low to high quality transcriptomes, we asked where in the graph a turning point could be identified (**fig. S1d**). In the density plot (**fig. S1d,** top panel), the three lines (blue, red, green) are the breakpoints where the slope of the density function (1^{st} derivative of density, **fig. S1d**, middle panel) has a sudden change. On the blue line, the downward slope (1st derivative) changes from being very steep to less steep, so that the 2^{nd} derivative is the highest at this point. Similarly, on the red line, the downward slope changes from less steep to more steep, so the 2^{nd} derivative is the lowest. Based on these observations, the three turning points were identified by the 2^{nd} derivative (**fig. S1d**, bottom panel). When a cutoff of 650 was applied, the number of molecule counts per cell was too low and the three DC populations – plasmacytoid DC (pDC) and conventional DC (cDC) subsets cDC1 and cDC2, could not be distinguished by principal component

analysis (PCA; **fig. S1e**). When a cutoff of 1,700 was applied, the number of cells retained was too low. Therefore, the 1,050 cutoff was an optimal tradeoff between the number of cells analyzed (cells retained after filtering by down sampling normalization) and the number of molecule counts in a cell (gene expression information that remains after discarding molecule counts by down sampling).

To ensure data reproducibility, stability and independence of the chosen molecule cutoff, we simulated our initial analyses using cutoffs of 650, 1,050, 1,700 and 2,350 molecule counts (**fig. S1e**). All four chosen simulation values exhibited the same general data topology if the data were dimensionally-reduced using PCA, thus proving that the biological data structure was robust and independent of filtering thresholds. In addition, we correlated the influence of the filtering threshold on the gene loadings within the first two principal components. Principal component 1 (PC1) of the dataset down-sampled to 1,050 molecule counts was highly correlated with PC1 of the datasets down-sampled to either 650 or 1,700 molecule counts (Pearson = 0.996 and 0.999, respectively). The same was true for PC2 (Pearson = 0.960 and 0.925, respectively). These results indicated that the chosen filtering cutoff of 1,050 was representative and objectively-derived.

The MARS-seq data obtained in this study were generated by two independent experiments (run1 and run2), which were combined for further data analysis. After normalization, the correlation between the average molecule count of all genes in run1 vs run2 was assessed (**fig. S1f**, which shows the high correlation between the average molecular counts in both runs (r=0.994)). When assessing for a batch effect, it is important to ensure that runs do not determine the clustering itself. We therefore plotted the t-distributed stochastic neighbor embedding (tSNE) values (**fig. S1g**) (cells of run1 and run2 in equal proportions) together with their density estimates. This analysis showed that the general distribution and, therefore, the clustering was not governed by the run, which is in line with the observation that our clustering identified biologically reasonable groups that clearly corresponded to the three DC populations (pDC, cDC1 and cDC2) (**Fig. 1A**). Consequently, the observed clusters were not explained by the variance between the runs, but by biology.

We next compared the frequencies of cell types, as determined by the clustering, within the two runs (**fig. S1h**). This showed that the ratio between the cells in different clusters was comparable between the two runs. Of note, the ratio does not need to be identical in both runs (*73*). In addition, this analysis showed that no cluster dominated a single run. Due to the fact that we are taking relatively small samples from a large total population, the frequencies of cell types are expected to show natural variation between runs, which could explain slight shifts in cellular frequencies.

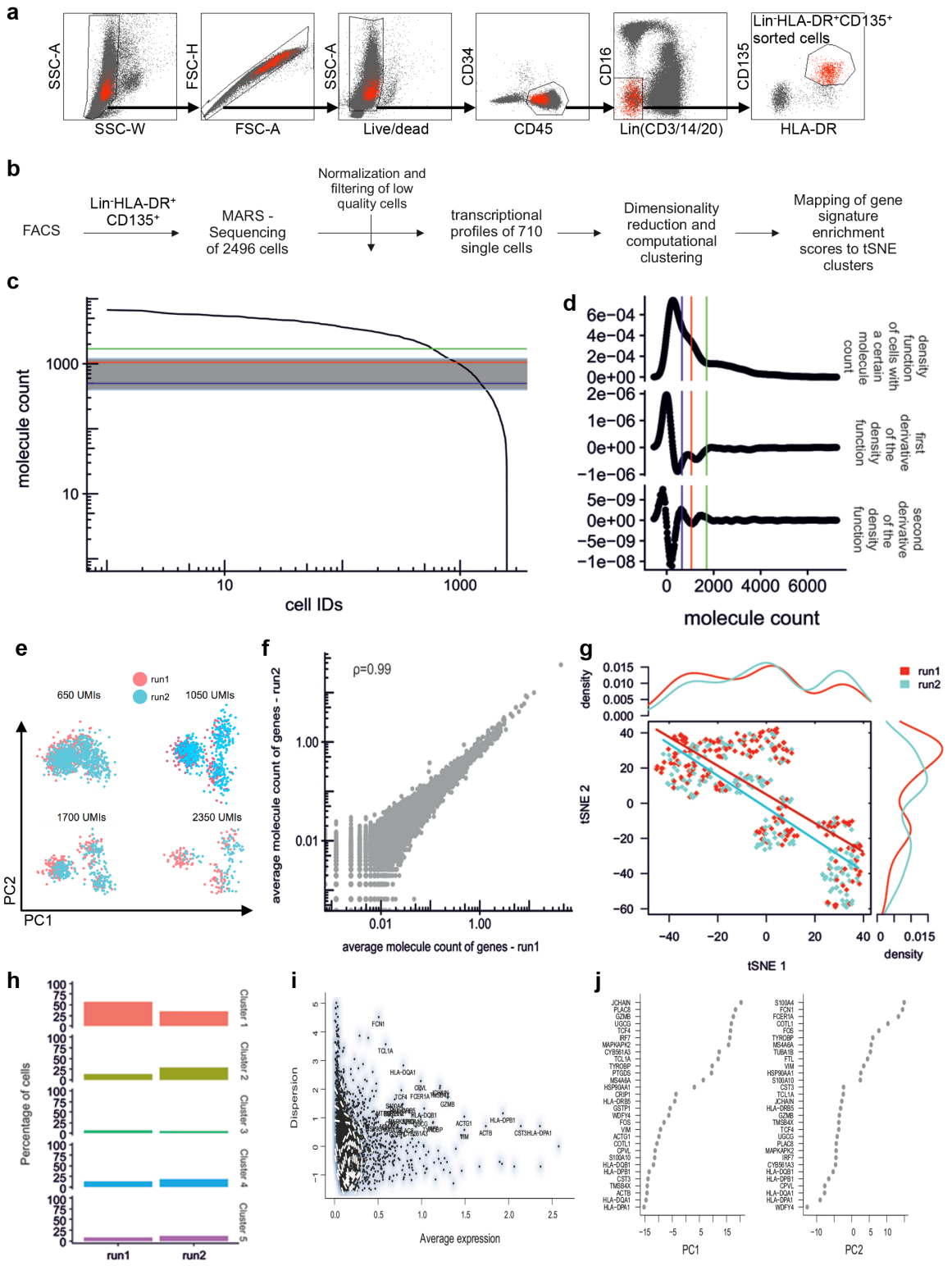

Fig. S1. **a**. Gating strategy for FACS of single cells from total Lin⁻HLA-DR⁺CD135⁺ cells. **b**. Workflow of the MARS-seq single cell data analysis. **c**. Association between molecule counts and cells. Cell IDs were sorted from highest to lowest number of unique

molecular identifier (UMI) or molecule counts. The data are presented on a log10 axis. The three colored lines correspond to molecule counts of 650 (blue), 1,050 (red) and 1,700 (green) per cell. The grey area indicates the range of molecule counts from 400 to 1,200 UMIs per cell. Cells with <1,050 molecules were removed from the analysis (n=1,786 cells). A total of 710 high-quality cells were used for further downstream analyses. **d.** Density plot (top panel) representing the distribution of cells with a certain number of molecules, and the first (middle panel) and second derivative (bottom panel) of the density function. The three colored lines correspond to molecule counts of 650 (blue), 1,050 (red) and 1,700 (green) per cell. **e.** Principal component analysis (PCA) after simulation at different normalization thresholds. Points were colored according to the different runs. **f.** Correlation plot of average expression of genes in run2 (y-axis) versus average expression of genes in run1 (x-axis). The data are presented on a log10 axis. The Pearson correlation coefficient was 0.99. **g.** t-distributed stochastic neighbor embedding (tSNE) analysis of the 710 single cells, colored by run association, showed an even distribution of the cells within the tSNE plot. Lines represent a linear fit of the points. The distributions of the points along the tSNE component 1 and component 2 were represented as density plots on the top or right panel, respectively. **h.** Frequency of cells in the five determined clusters for run1 and run2. **i.** Mean-variability plot showed average expression and dispersion for each gene. This analysis was used to determine highly variable gene expression (labeled by gene symbol). The 36 highly variable genes were used to perform a dimensionality reduction of the single-cell data by PCA. **j.** The highest gene loadings in the first and second principal component (PC1 and PC2) from the PCA of 710 high quality cells are shown.

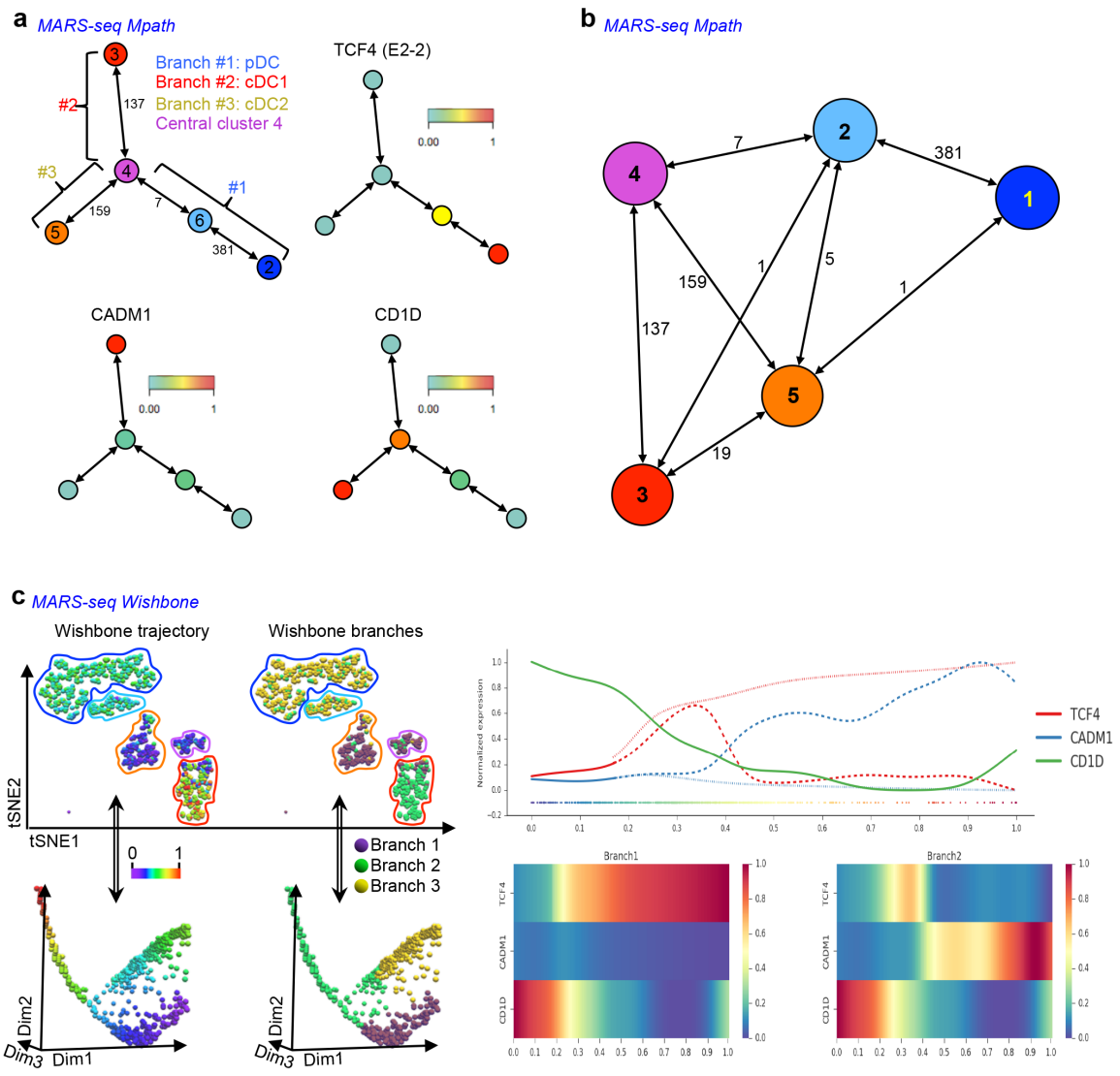

Fig. S2. a. Relative expression of signature genes of pDC (TCF4), cDC1 (CADM1) and cDC2 (CD1D) in Mpath clusters defined in Fig. 1C. **b.** Weighted neighborhood network of the Mpath analysis shown in Fig. 1C. **c.** Analysis of MARS-seq data using the Wishbone algorithm. In the 2D-t-distributed stochastic neighbor embedding (tSNE) plot (upper panels) and in the 3D-Diffusion Map (lower panels) (See Fig. 1, A and F, respectively), cells were colored according to the values of the Wishbone trajectory (left panels) or the values of the Wishbone branches (right panels). Line chart (top right panel) of expression of signature genes along Wishbone trajectory. X-axis represents pseudo-

time of Wishbone trajectory. Solid line represents backbone trajectory, dotted lines represent separate trajectories along the two branches. Heat maps (bottom right panels) of expression of signature genes along Wishbone trajectory on the two branches.

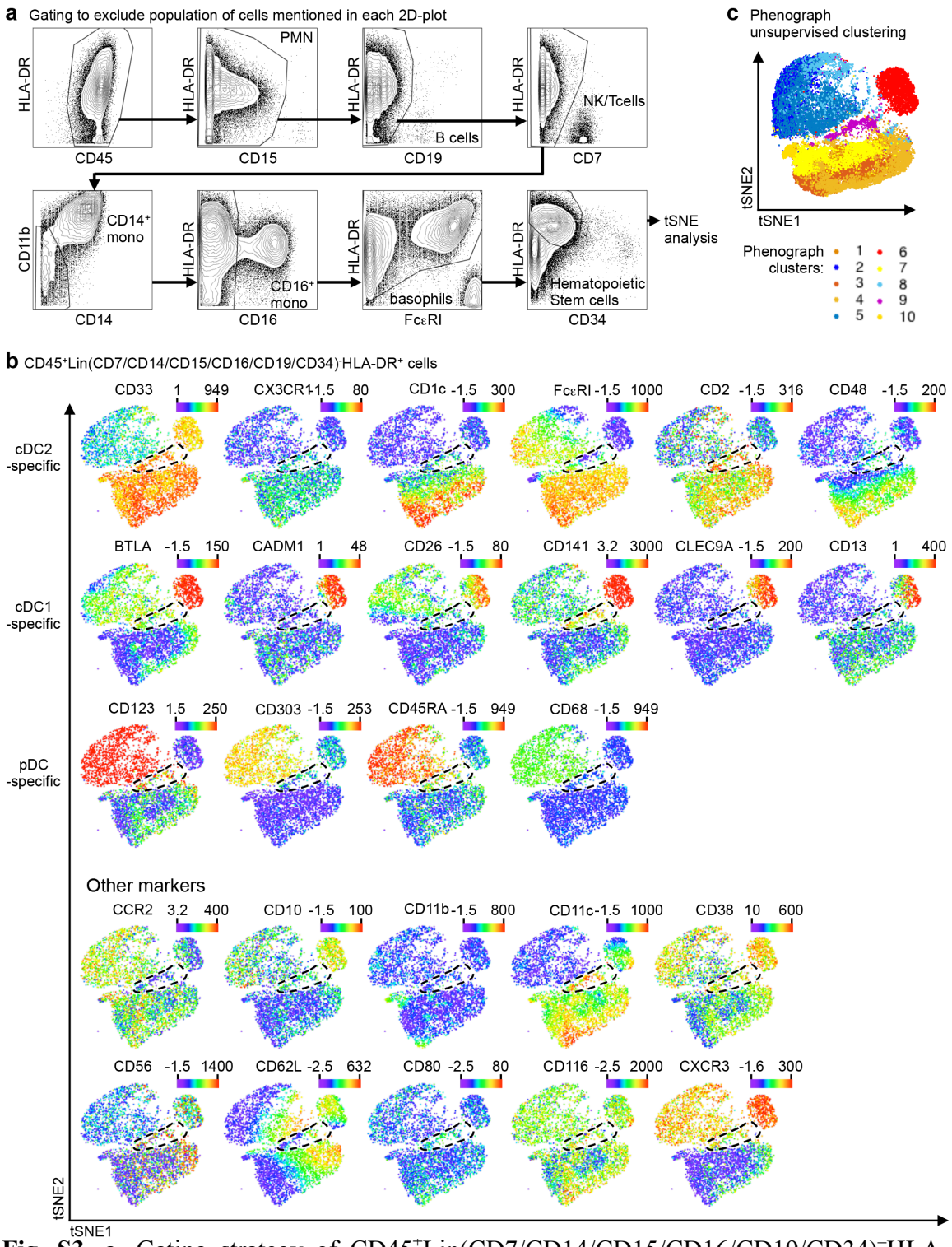

Fig. S3. **a.** Gating strategy of $CD45^{+}Lin(CD7/CD14/CD15/CD16/CD19/CD34)^{-}HLA\text{-}DR^{+}$ blood mononuclear cells from CyTOF analysis for downstream t-distributed stochastic neighbor embedding (tSNE) as shown in Fig. 1, E to G. The name of the

excluded population(s) is indicated in each corresponding 2D-plot. **b.** tSNE plots of the CyTOF data from Fig. 1, H to J showing the expression level of cDC2-, cDC1- and pDC-specific markers. **c.** Unsupervised phenograph clustering identified 10 clusters that were overlaid onto the tSNE1/2 plot of the CyTOF data from Fig. 1, H and I.

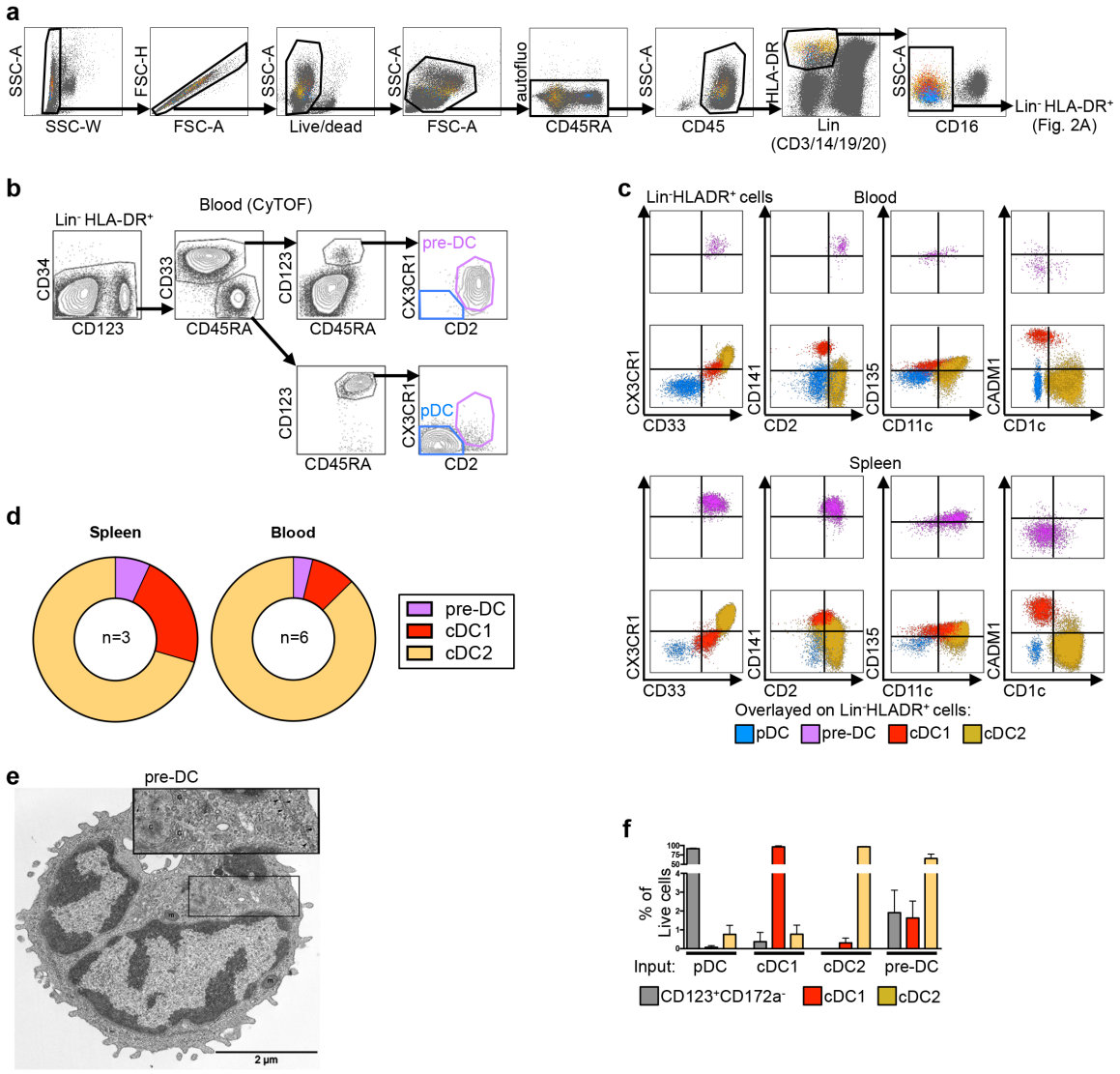

Fig. S4. **a.** Gating of flow cytometry data to identify the Lin$^-$HLA-DR$^+$ cell population displayed in Fig. 2A (blood data displayed). **b.** Classical contour plots of CyTOF data from Fig. 1 showing the same gating strategy as applied in the flow cytometry analyses shown in Fig. 2A. **c.** Flow cytometry data showing the relative expression of CD33, CX3CR1, CD2, CD141, CD11c, CD135, CD1c and CADM1 by pre-DC, pDC, cDC1 and cDC2 defined in Fig. 2A in the blood (upper panels) and spleen (lower panels). **d.** Ring graphical representation of the proportion of pre-DC, cDC1 and cDC2 among total Lin$^-$

$CD34^{-}HLA\text{-}DR^{+}CD33^{+}$ cDC defined in Fig. 2A in the spleen (left) and blood (right). **e.** Representative electron micrographs showing morphological characteristics of a pre-DC. **f.** Histograms of the mean relative numbers of $CD123^{+}CD172\alpha^{-}$ cells, $Clec9A^{+}CADM1^{+}$ cDC1 or $CD172\alpha^{+}CD1c^{+}$ cDC2 from the *in vitro* differentiation assays as described in Fig. 2F (n=4). Error bars represent mean ± SEM.

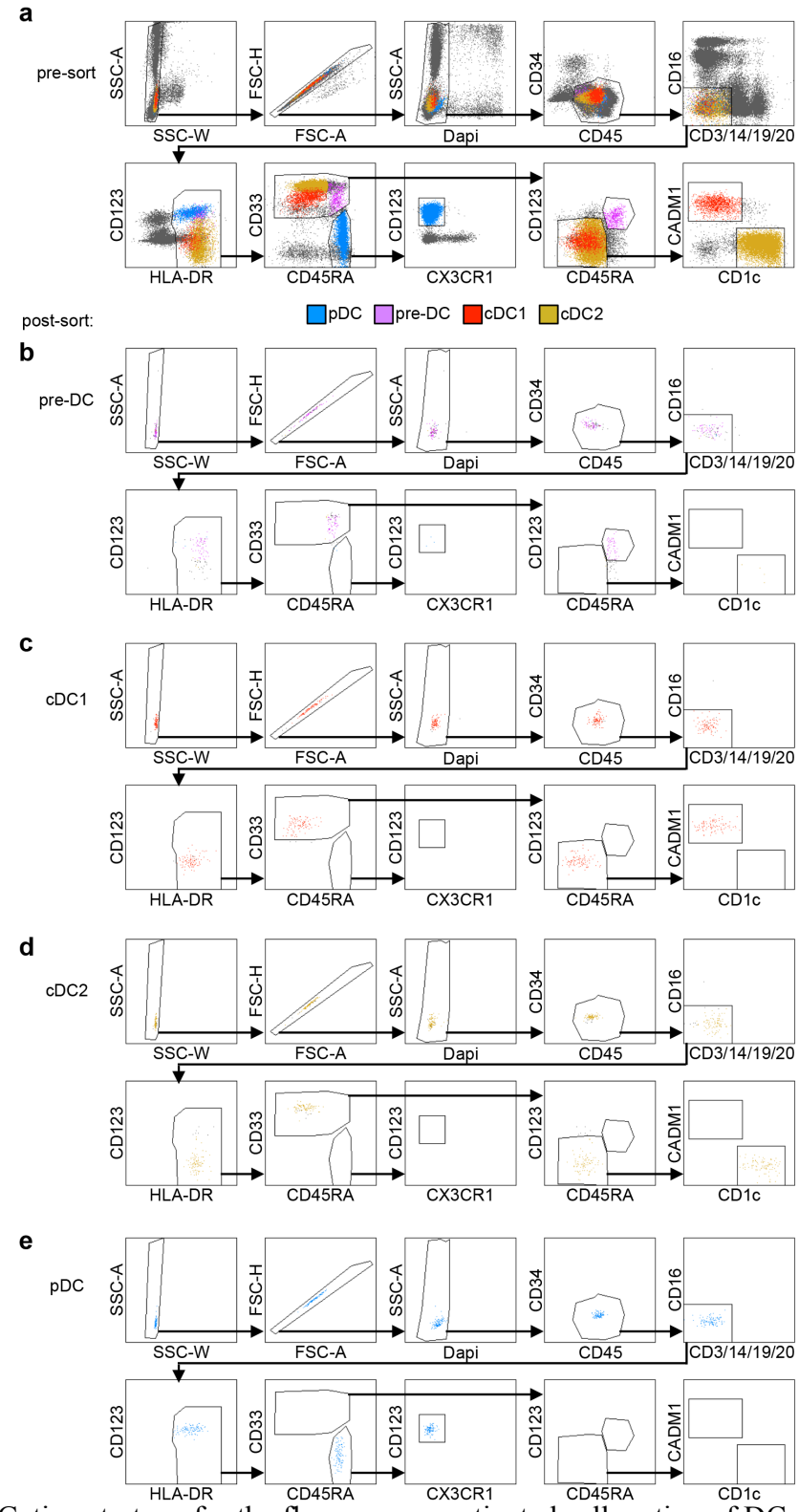

Fig. S5. Gating strategy for the fluorescence-activated cell sorting of DC subsets and pre-DC used in the *in vitro* differentiation assays (Fig. 2F). **a.** Pre-sorted data and **b-d.** post-sorted re-analysis of **b.** pre-DC, **c.** cDC1, **d.** cDC2, and **e.** pDC.

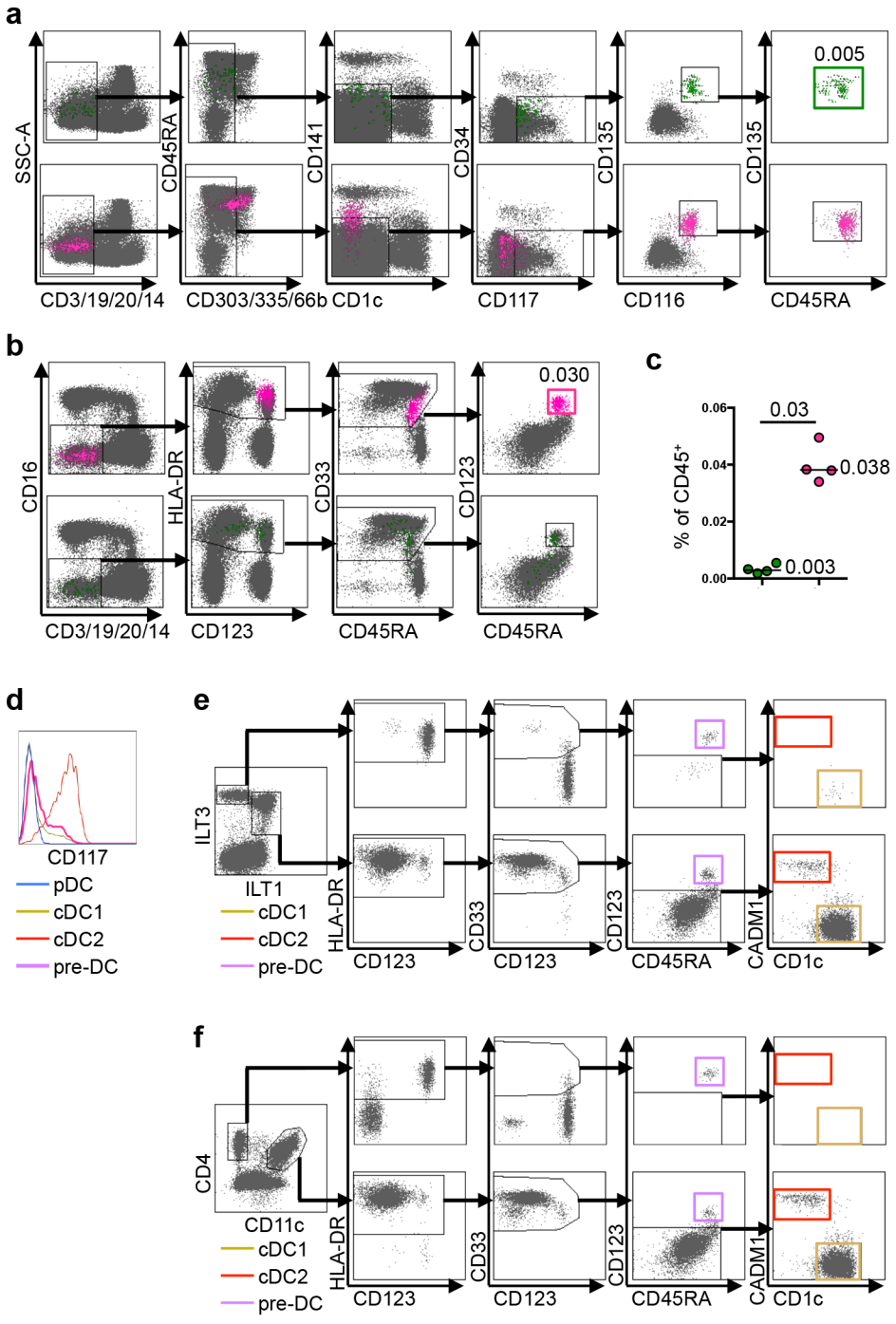

Fig. S6. **a-c.** Comparison of **a.** the gating strategy from Breton *et al.* (*9*) pre-DC are shown in green) and **b.** the gating strategy used in Fig. 2A and fig. S4a (pre-DC displayed in purple) to define pre-DC. The relative numbers of pre-DC defined using the two gating strategies among live $CD45^+$ peripheral blood mononuclear cells are indicated in the dot

plots. **c.** Graphical representation of the median relative numbers of pre-DC defined using the two gating strategies among live $CD45^+$ blood mononuclear cells (n=4). The median percentages of $CD45^+$ values are indicated. P-values were calculated using the Mann-Whitney test. **d.** Histogram showing the expression of CD117 by DC subsets and pre-DC determined by flow cytometry. **e-f.** Identification of pre-DC (purple gate), cDC1 (red gate) and cDC2 (beige gate) among $Lin^-HLA\text{-}DR^+$ **e.** $ILT3^+ILT1^-$ cells (*10*) or $ILT3^+ILT1^+$ (cDC), and **f.** $CD4^+CD11c^-$ cells (*11*) or $CD4^{int}CD11c^+$ cDC. .

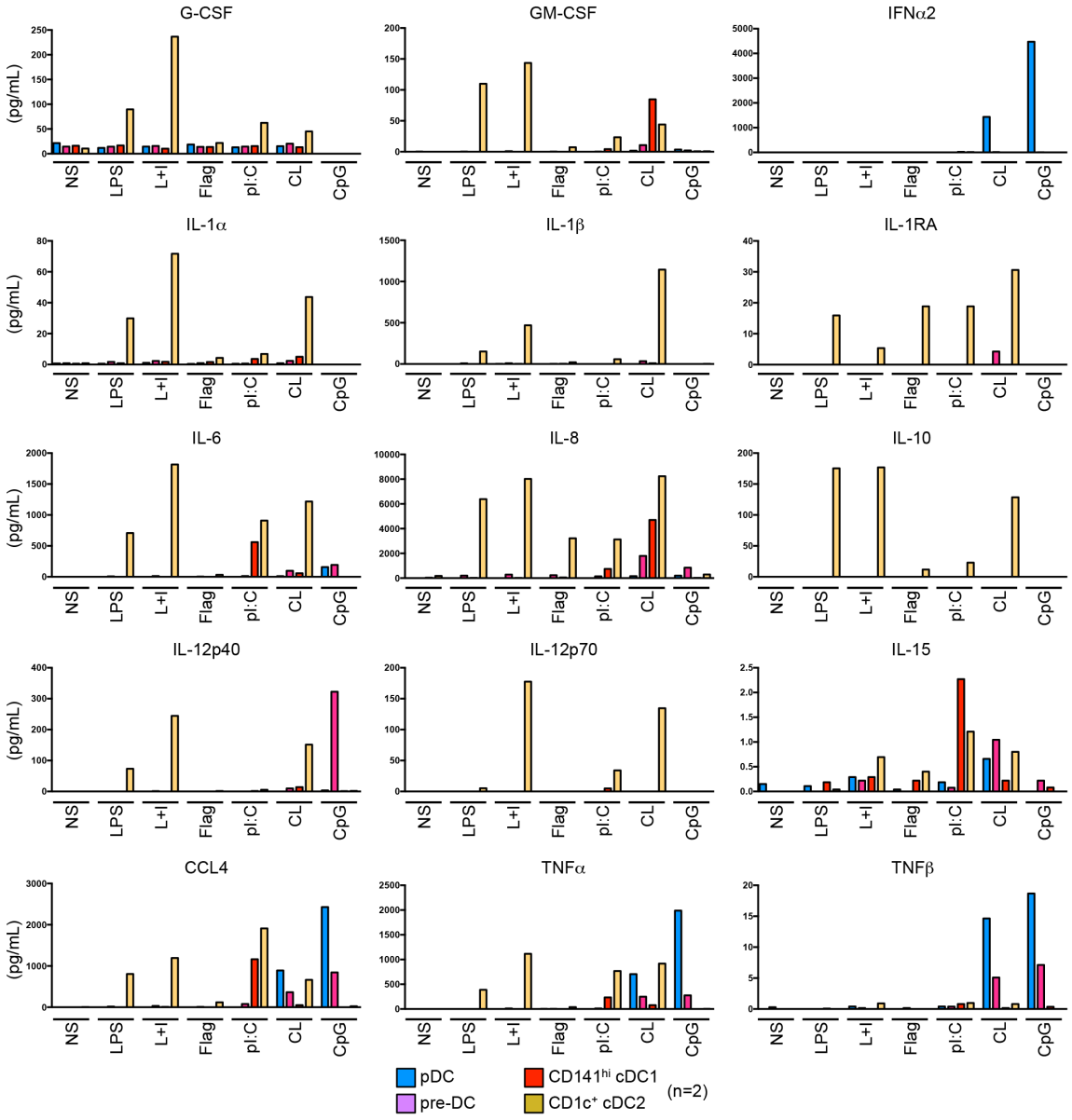

Fig. S7. pDC, pre-DC, cDC1 and cDC2 isolated by fluorescence-activated cell sorting were stimulated *in vitro* with LPS, LPS+IFNγ (L+I), Flagellin (Flag), polyI:C (pI:C), CL097 (CL) or CpG ODN2216 (CpG), and the soluble mediators (as indicated above each histogram) in the culture supernatants were quantified by Luminex Multiplex Assay (n=2).

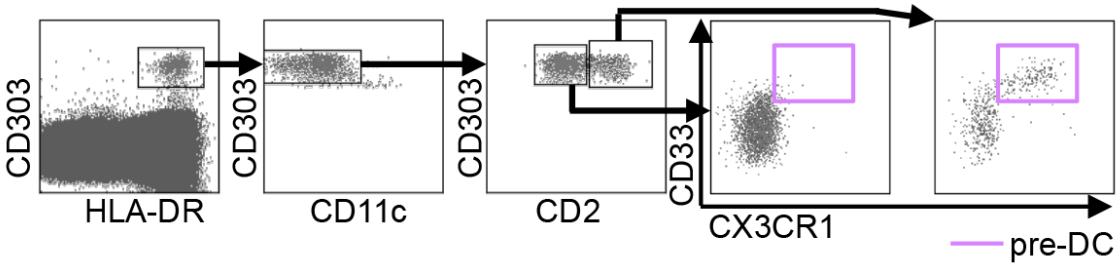

Fig. S8. Identification of $CD33^{+}CX3CR1^{+}$ pre-DC among $Lin^{-}HLA\text{-}DR^{+}CD303^{+}CD2^{+}$ cells (*34*).

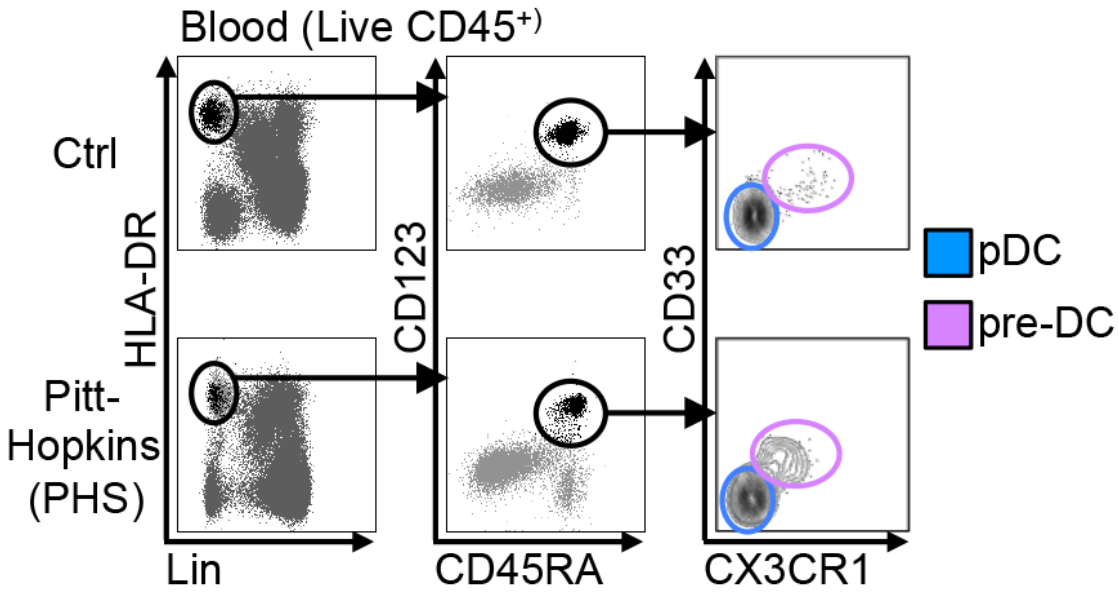

Fig. S9. Gating strategy for the fluorescence-activated cell sorting analysis of peripheral blood mononuclear cells from control subjects (Ctrl, n=11) and patients with Pitt-Hopkins Syndrome (PHS; n=4). pDC (circled in blue) and pre-DC (circled in purple) were defined among Lin-HLA-DR^{+}CD45RA^{+}CD123^{+} cells.

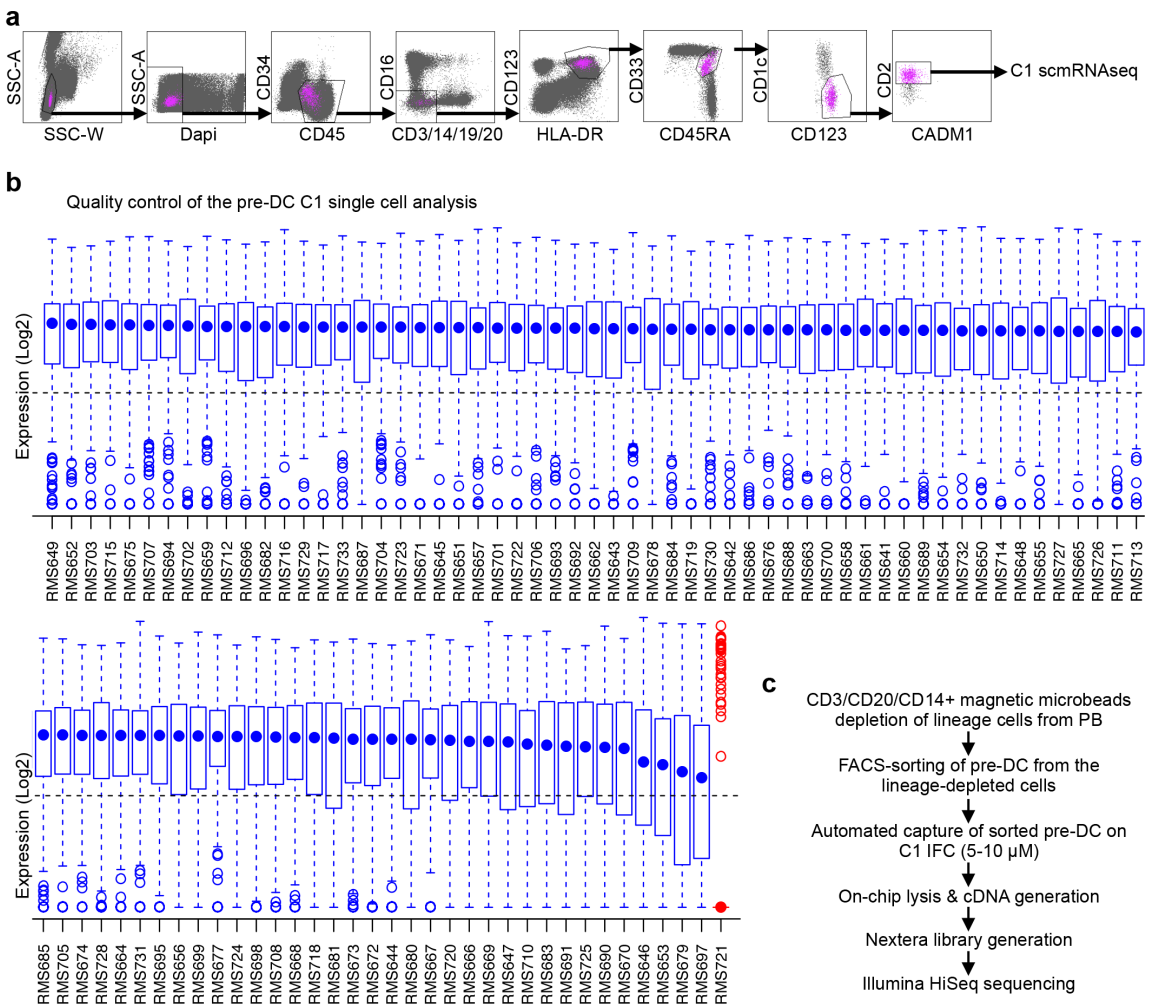

Fig. S10. **a.** Gating strategy for FACS of Lin$^-$HLA-DR$^+$CD33$^+$CD45RA$^+$CD1c$^{lo/-}$CD2$^+$CADM1$^{lo/-}$CD123$^+$ pre-DC analyzed by C1 single cell mRNA sequencing (scmRNAseq). **b.** Quality control (removing low-quality cells and minimally-expressed genes below the limits of accurate detection; low-quality cells that were identified using SINGuLAR toolbox; minimally-expressed genes with transcripts per million (TPM) values ≥1 in <95% of the cells) and **c.** work flow of the C1 scmRNAseq analyses shown in Fig. 3A-B. Error bars represent the maximum, third quartile, median, first quartile and minimum.

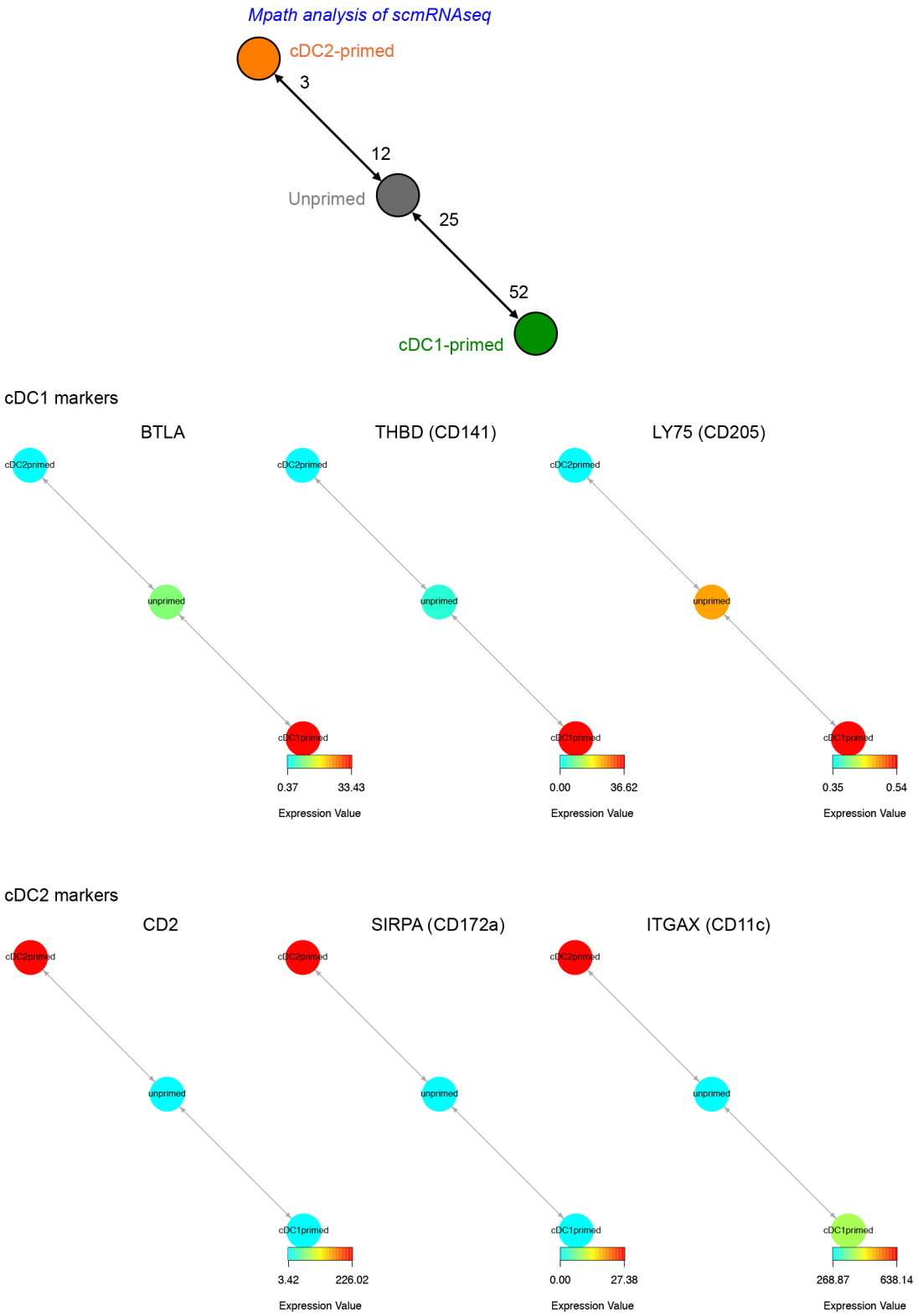

Fig. S11. Relative expression levels of signature genes of cDC1 (BTLA, THBD and, LY75) and cDC2 (CD2, SIRPA and ITGAX) in Mpath clusters defined in Fig. 3B.

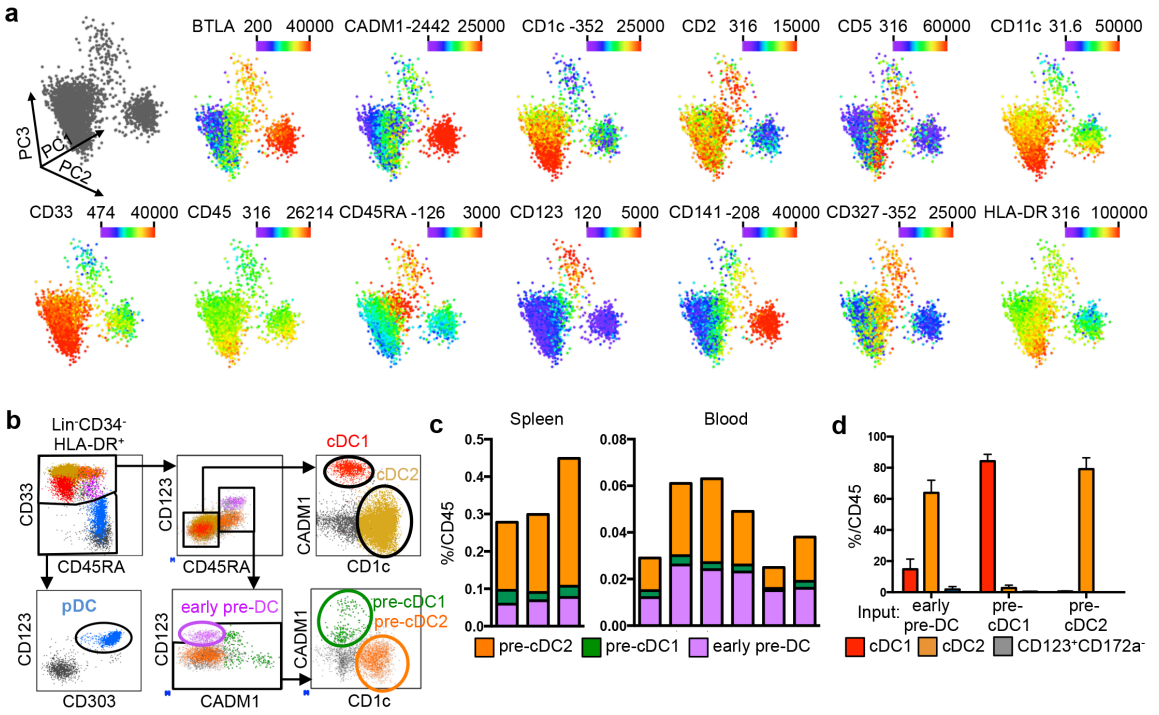

Fig. S12. **a.** Expression level of markers in the 3D-Principal Component Analysis (PCA) plots from Fig. 3, C and D are shown. **b.** Sequential gating strategy of flow cytometry data starting from Live $CD45^+Lin(CD3/14/16/19/20)^-CD34^-HLA\text{-}DR^+$ peripheral blood mononuclear cells defining $CD33^-CD123^+CD303^+$ pDC, $CD33^+CD45RA^-$ differentiated cDC ($CADM1^+$ cDC1, $CD1c^+$ cDC2), and $CD33^+CD45RA^+$ cells (comprising $CD123^+CD45RA^+$ pre-DC and $CD123^{lo}CD45RA^+$ intermediate cells). **c.** Proportion of $CD45^+$ mononuclear cells in spleen (n=3) (left) and peripheral blood (n=6) (right) of the above-mentioned pre-DC subsets. **d.** Histograms of the mean proportion of $CD303^+CD172\alpha^-$ cells, $Clec9A^+CADM1^+$ cDC1 or $CD1c^+CD11c^+$ cDC2 obtained in the *in vitro* differentiation assays as described in Fig. 3H (n=3). Error bars represent mean ± SEM.

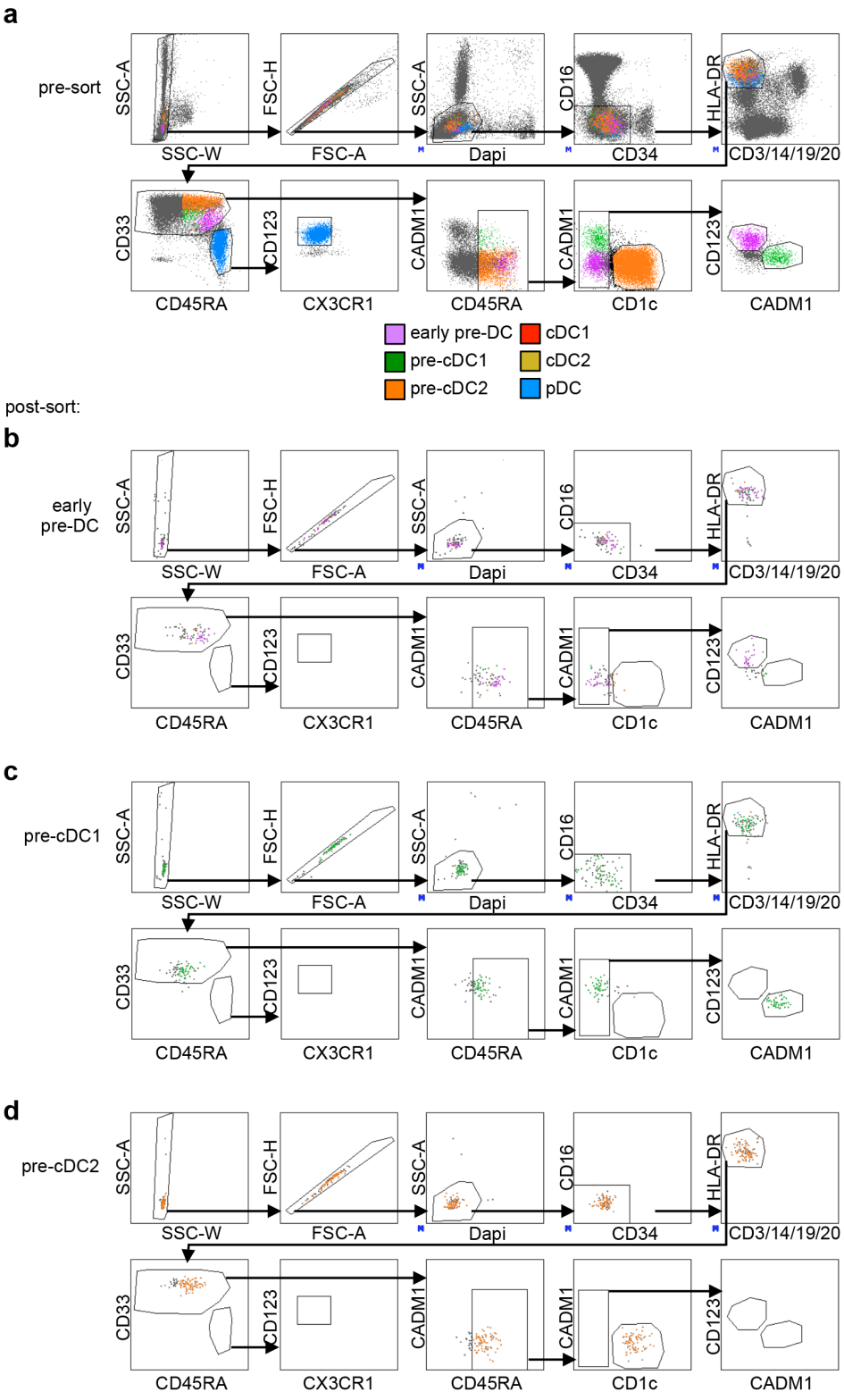

Fig. S13. Gating strategy for sorting of pre-DC subsets used in the *in vitro* differentiation assays (Fig. 3G). **a.** Pre-sorted data and **b-d.** post-sorted re-analysis of **b.** early pre-DC, **c.** pre-cDC1, and **d.** pre-cDC2 are shown.

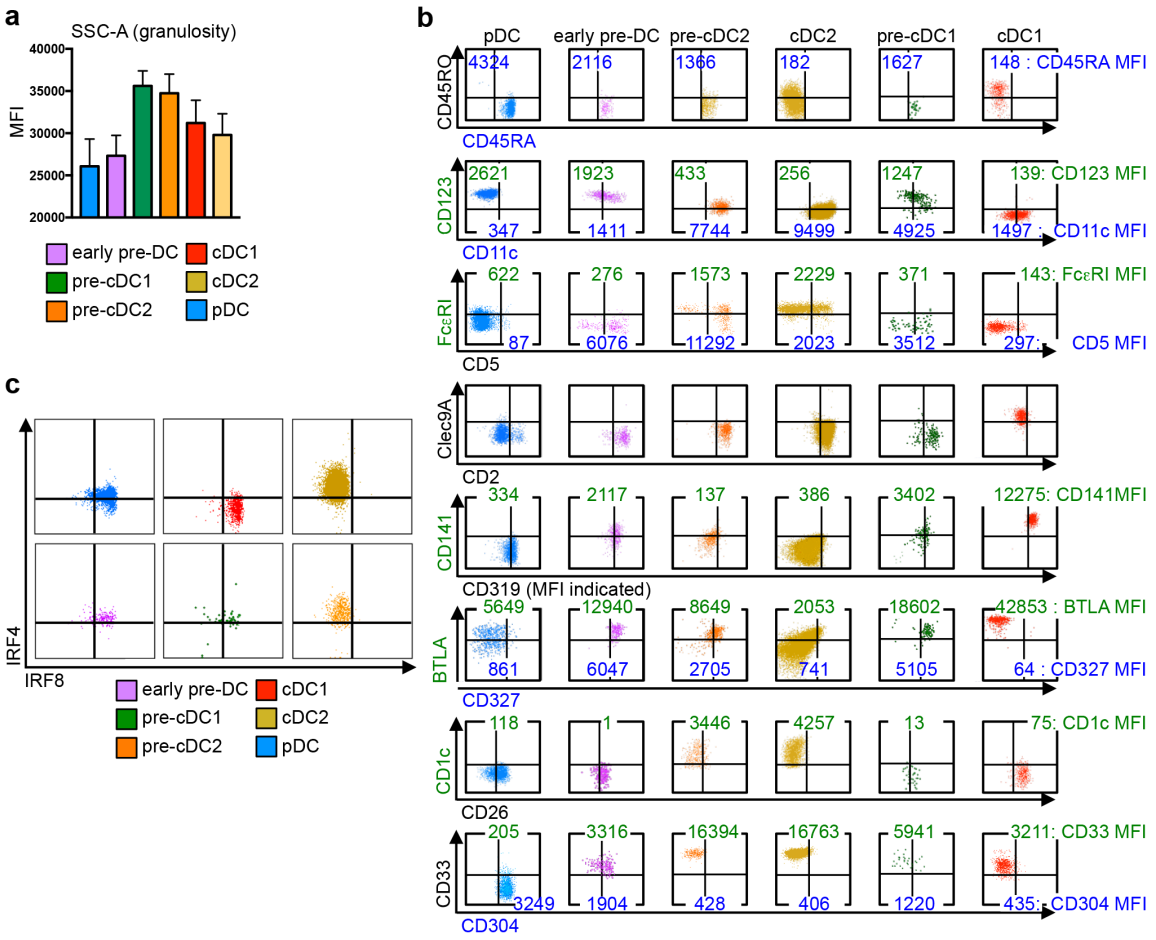

Fig. S14. **a.** Expression level in terms of mean fluorescence intensity (MFI) of the side scatter area (SSC-A) indicating cellular granularity of blood pre-DC and DC subsets from five individual human donors (n=5) Error bars represent mean ± SEM.. **b-c.** Flow cytometry data showing the relative expression of **b.** CD45RA, CD169, CD11c, CD123, CD33, FcεRI, CD2, Clec9A, CD319, CD141, BTLA, CD327, CD26, CD1c, CD304 or of **c.** IRF4 and IRF8 by pDC, early pre-DC, pre-cDC2, cDC2, pre-cDC1 and cDC1 defined in Fig. 3G and in fig. S12b.

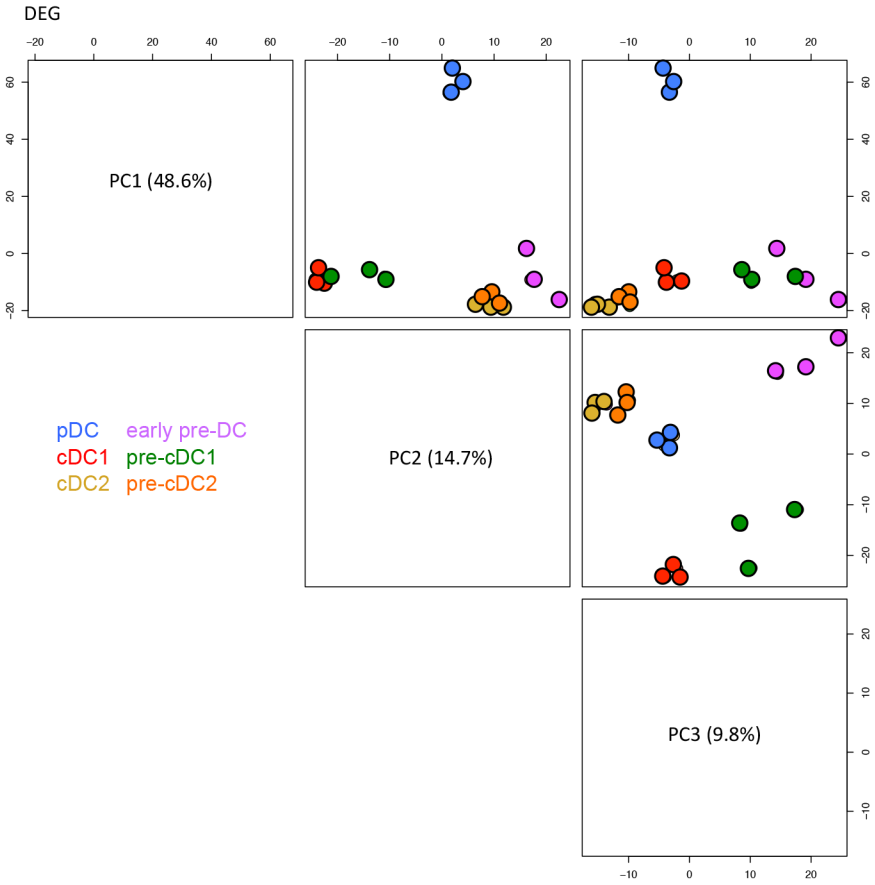

Fig. S15. 2D-plots showing combinations of Principal Component Analysis components 1, 2 or 3 (PC1-3) using differentially-expressed genes from the microarray analysis of Fig. 4.

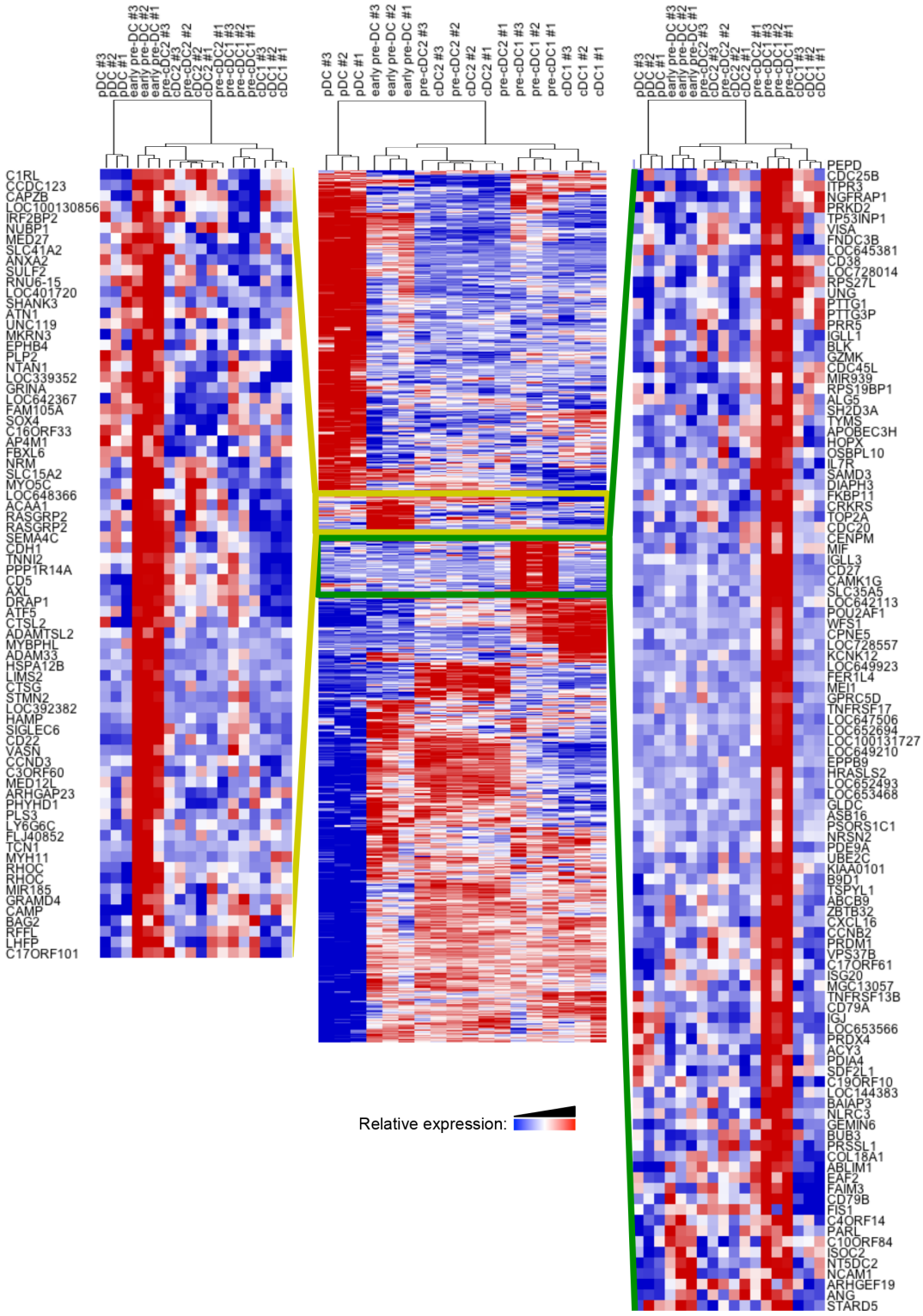

Fig. S16. Heat maps of relative expression levels of all differentially-expressed genes, with magnifications of the specific genes in early pre-DC (boxed yellow region) and pre-cDC1 (boxed green region) from the microarray analysis of Fig. 4.

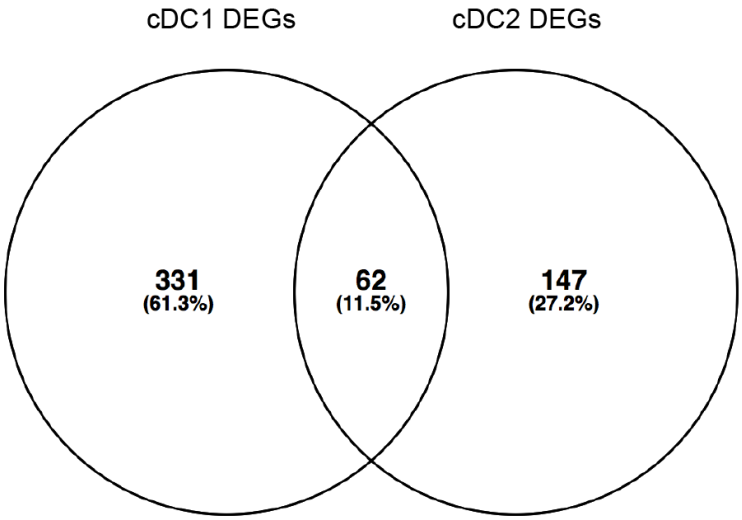

Fig. S17. Venn diagram showing genes common between the lists of cDC1 DEGs (the union of DEGs from comparing pre-cDC1 vs early pre-DC and cDC1 vs pre-cDC1) and cDC2 DEGs (the union of DEGs from comparing pre-cDC2 vs early pre-DC and cDC2 vs pre-cDC2). These 62 genes were then plotted in Fig. 4E with the log2 fold-change values (versus early pre-DC).

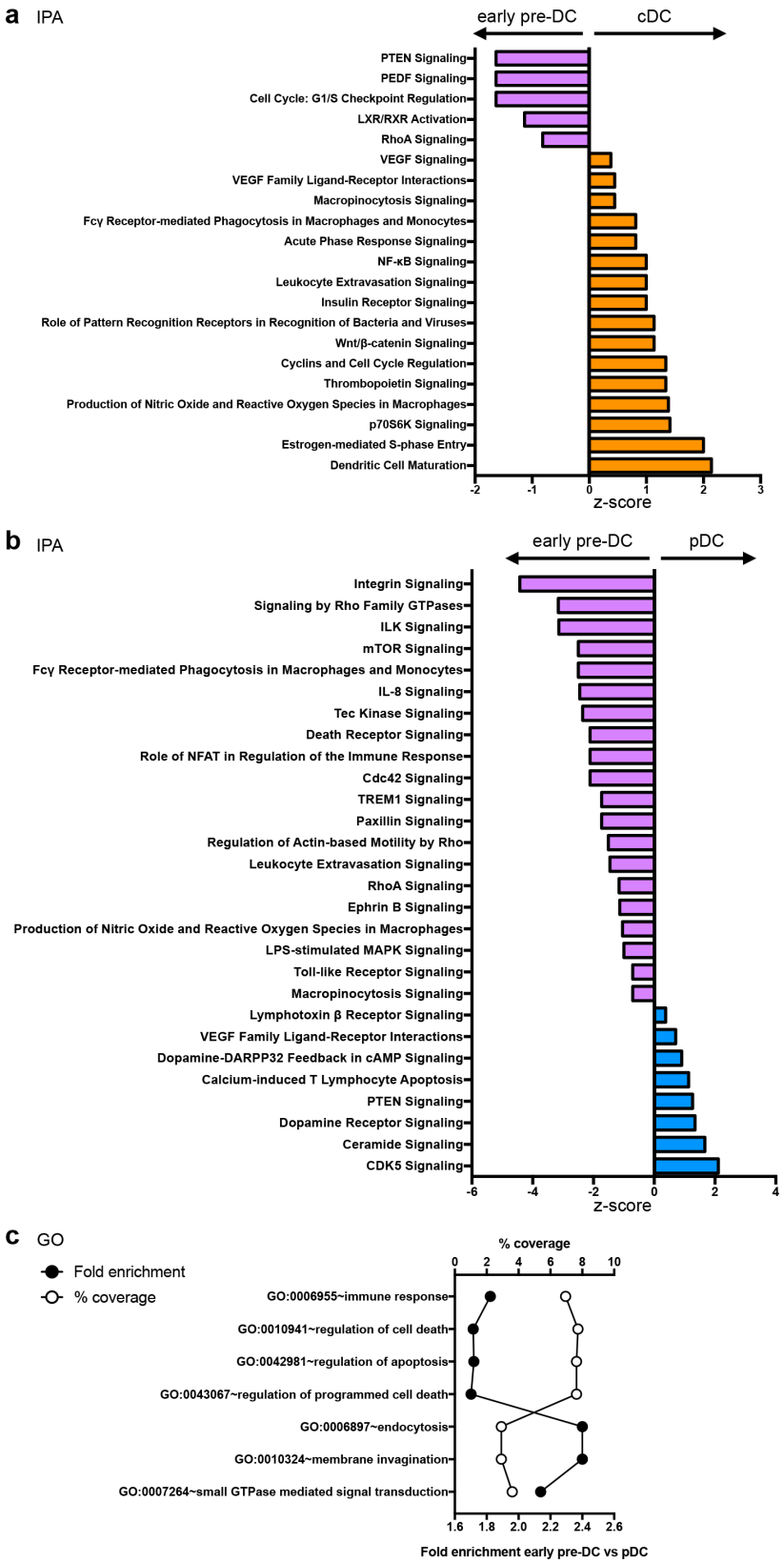

Fig. S18. **a-b.** Ingenuity Pathway analysis (IPA) based on genes that were differentially-expressed between **a.** cDC and early pre-DC or **b.** pDC and early pre-DC. Only the DC

biology-related pathways were shown, and all displayed pathways were significantly enriched ($P<0.05$, right-tailed Fischer's Exact Test). The heights of the bars correspond to the activation z-scores of the pathways. Enriched pathways predicted to be more activated in early pre-DC pathways are shown in pink and enriched pathways predicted to be more activated in cDC or pDC are shown in orange and blue, respectively. IPA predicts pathway activation/inhibition based on the correlation between what is known about the pathways in the literature (the Ingenuity Knowledge Base) and the directional expression observed in the user's data. Please refer to IPA Upstream Regulator Analysis Whitepaper and IPA Downstream Effectors Analysis Whitepaper for full description of the activation z-score calculation. **c.** Gene Ontology (GO) enrichment analysis of differentially-expressed genes (DEGs) in early pre-DC and pDC indicating biological processes that were significantly enriched (Benjamini-Hochberg adjusted p value < 0.05) with genes expressed more abundantly in early pre-DC as compared to pDC. Note that no biological process was significantly enriched with genes expressed more abundantly in pDC as compared to early pre-DC.

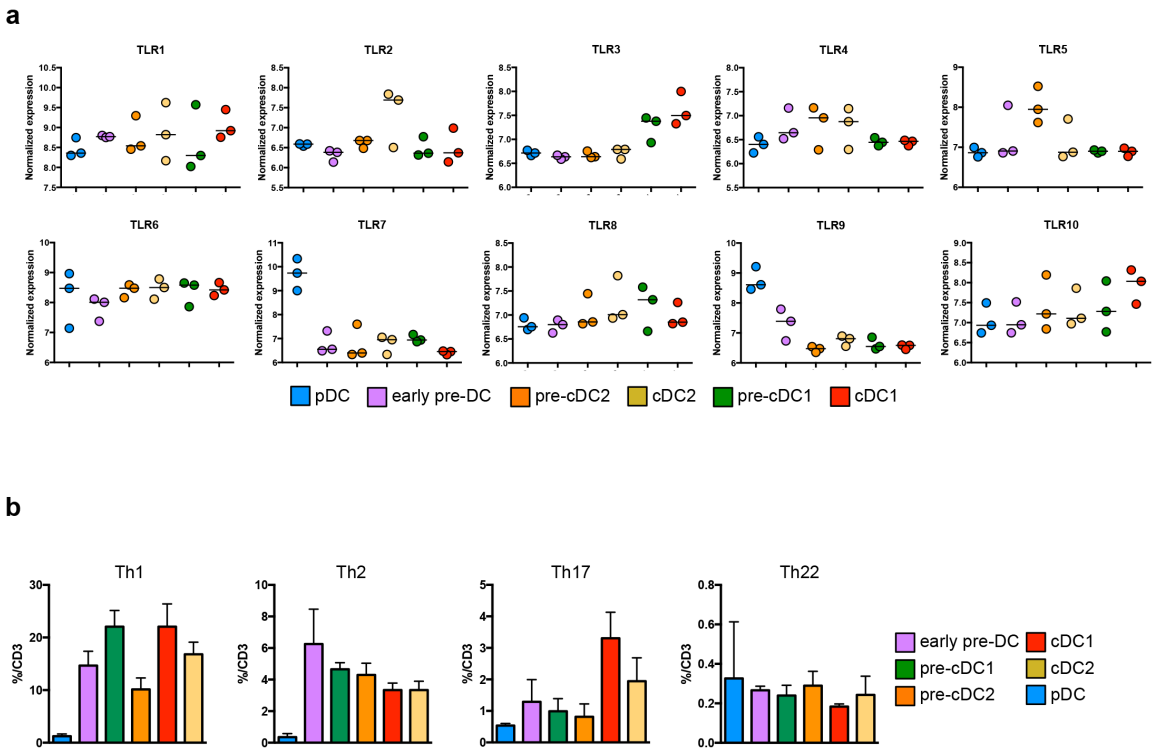

Fig. S19. **a.** Normalized abundance of all TLR mRNA in DC and pre-DC subsets obtained from the microarray analysis of Fig. 4. **b.** Polarization of naïve $CD4^+$ T cells into $IFN\gamma^+IL\text{-}17A^-$ Th1 cells, $IL\text{-}4^+$ Th2 cells, $IL17A^+IFN\gamma^-$ Th17 cells and $IL\text{-}22^+IFN\gamma^-$ $IL\text{-}17A^-$ Th22 cells after 6 days of culture in a mixed lymphocyte reaction with allogenic pre-DC and DC subsets (n=3). Error bars represent mean ± SEM.

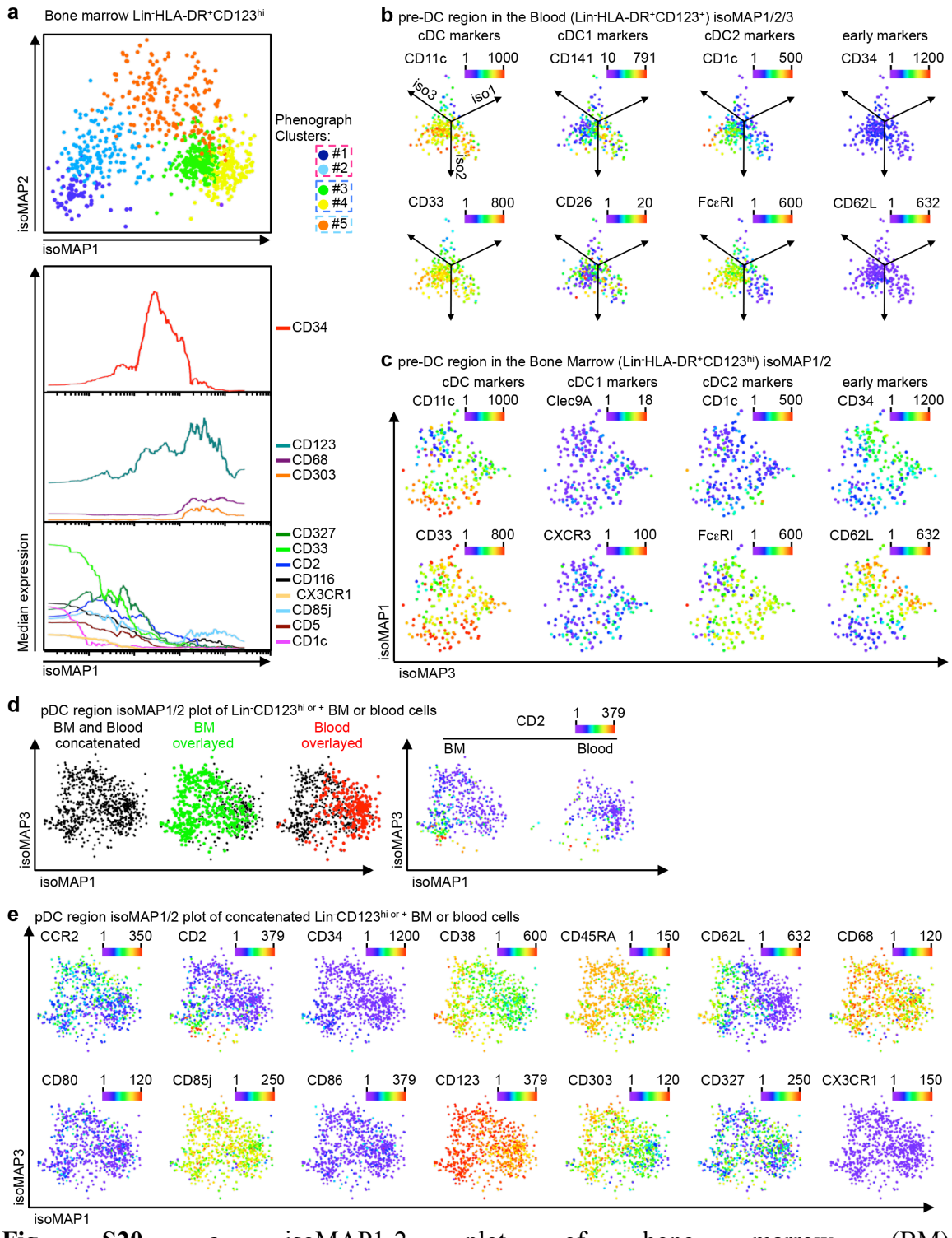

Fig. S20. **a.** isoMAP1-2 plot of bone marrow (BM) Lin(CD3/CD7/CD14/CD15/CD19/CD34)$^{-}$CD123^{hi} cells (upper panel) and graphics of the binned median expression of defining markers along the phenotypic progression of cells

defined by the isoMAP1 dimension (lower panels) are shown. **b.** Expression level of selected markers in the isoMAP1-2-3 3D-plots (Fig. 6C, lower left panel) corresponding to cells within the pre-DC phenograph clusters (#1 and #2) of the blood $Lin^{-}CD123^{+}$ cells isoMAP analysis. **c.** Expression level of selected markers in the isoMAP1-2 plots (Fig. 6C, upper left panel) corresponding to cells within the pre-DC phenograph clusters (#3 and #4) of the BM $Lin^{-}CD123^{hi}$ cells isoMAP analysis. **d.** pDC defined in BM $Lin^{-}CD123^{hi}$ (green: phenograph clusters #3 and #4) or blood $Lin^{-}CD123^{+}$ (red: phenograph cluster #7) cells of Fig. 6A and 6B, respectively, were exported and analyzed using the isoMAP method and subdivided into clusters using the phenograph algorithm. BM and blood concatenated (black) and overlaid BM (green) and blood (red) isoMAP1/3 plots are shown (left panels). Expression level of CD2 in BM (left) and blood (right) pDC in the isoMAP1/3 plot. **e.** Expression level of selected markers in the BM and blood concatenated isoMAP1/3 plot of Fig. 6C (right panels).

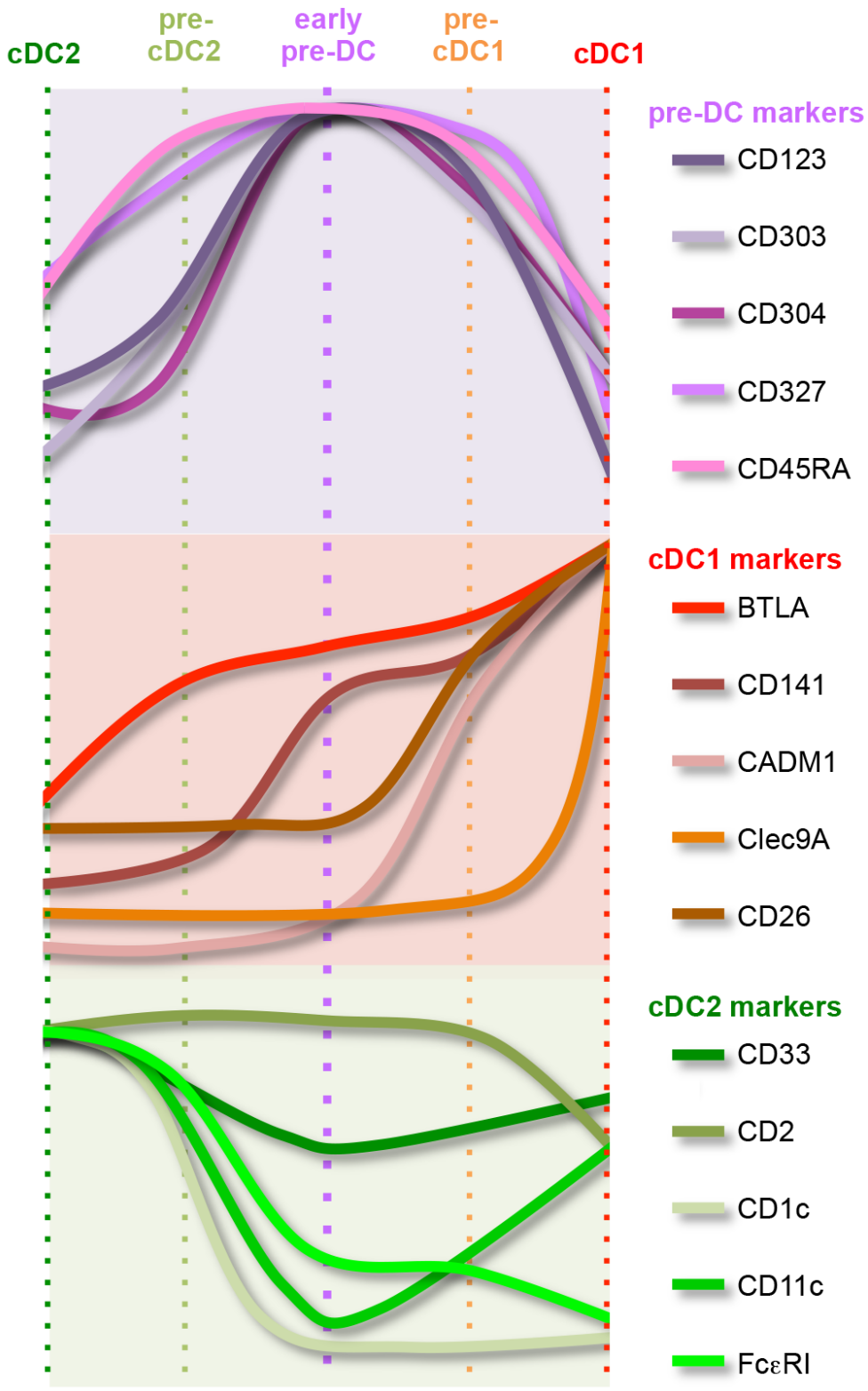

Fig. S21. Schematic representation of the expression of major pre-DC, cDC1 and cDC2 markers as pre-DC differentiate towards cDC.

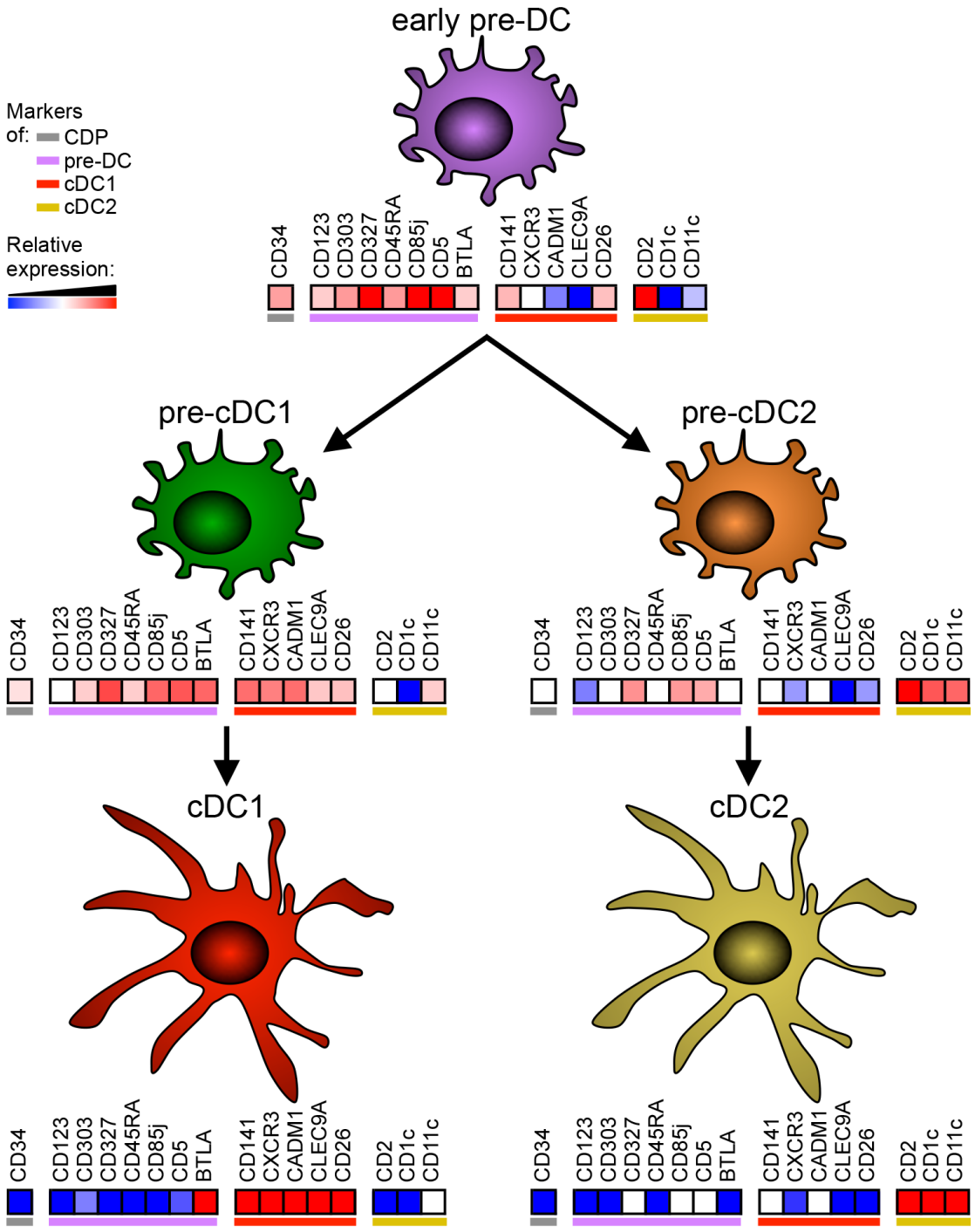

Fig. S22. Schematic representation of the expression of major pre-DC, cDC1 and cDC2 markers as pre-DC differentiate towards cDC.

Supplementary Tables S1-S16 are provided online as a separate file:

Table S1. Number of detected genes per cell in the total DC MARS-seq experiment

Table S2. DC subsets signature genes derived from Gene Expression Omnibus data series GSE35457 and used for MARS-seq and C1 data analyses

Table S3. List of anti-human antibodies used for mass cytometry (CyTOF)

Table S4. Number of expressed genes detected per cell in the pre-DC C1 scmRNAseq experiment

Table S5. Lists of genes identified from the microarray DEG analysis comparisons along the lineage progression from early pre-DC to mature cDC, for cDC1 and cDC2 respectively, and the list of the 62 common genes

Table S6. List of anti-human antibodies used for flow cytometry

References

1. A. Schlitzer, N. McGovern, F. Ginhoux, Dendritic cells and monocyte-derived cells: Two complementary and integrated functional systems. *Semin. Cell Dev. Biol.* **41**, 9–22 (2015). doi:10.1016/j.semcdb.2015.03.011 Medline

2. M. Merad, P. Sathe, J. Helft, J. Miller, A. Mortha, The dendritic cell lineage: Ontogeny and function of dendritic cells and their subsets in the steady state and the inflamed setting. *Annu. Rev. Immunol.* **31**, 563–604 (2013). doi:10.1146/annurev-immunol-020711-074950 Medline

3. M. Guilliams, F. Ginhoux, C. Jakubzick, S. H. Naik, N. Onai, B. U. Schraml, E. Segura, R. Tussiwand, S. Yona, Dendritic cells, monocytes and macrophages: A unified nomenclature based on ontogeny. *Nat. Rev. Immunol.* **14**, 571–578 (2014). doi:10.1038/nri3712 Medline

4. K. Liu, G. D. Victora, T. A. Schwickert, P. Guermonprez, M. M. Meredith, K. Yao, F. F. Chu, G. J. Randolph, A. Y. Rudensky, M. Nussenzweig, In vivo analysis of dendritic cell development and homeostasis. *Science* **324**, 392–397 (2009). Medline

5. F. Ginhoux, K. Liu, J. Helft, M. Bogunovic, M. Greter, D. Hashimoto, J. Price, N. Yin, J. Bromberg, S. A. Lira, E. R. Stanley, M. Nussenzweig, M. Merad, The origin and development of nonlymphoid tissue CD103+ DCs. *J. Exp. Med.* **206**, 3115–3130 (2009). doi:10.1084/jem.20091756 Medline

6. N. Onai, K. Kurabayashi, M. Hosoi-Amaike, N. Toyama-Sorimachi, K. Matsushima, K. Inaba, T. Ohteki, A clonogenic progenitor with prominent plasmacytoid dendritic cell developmental potential. *Immunity* **38**, 943–957 (2013). doi:10.1016/j.immuni.2013.04.006 Medline

7. A. Schlitzer, V. Sivakamasundari, J. Chen, H. R. B. Sumatoh, J. Schreuder, J. Lum, B. Malleret, S. Zhang, A. Larbi, F. Zolezzi, L. Renia, M. Poidinger, S. Naik, E. W. Newell, P. Robson, F. Ginhoux, Identification of cDC1- and cDC2-committed DC progenitors reveals early lineage priming at the common DC progenitor stage in the bone marrow. *Nat. Immunol.* **16**, 718–728 (2015). doi:10.1038/ni.3200 Medline

8. J. Lee, G. Breton, T. Y. K. Oliveira, Y. J. Zhou, A. Aljoufi, S. Puhr, M. J. Cameron, R.-P. Sékaly, M. C. Nussenzweig, K. Liu, Restricted dendritic cell and monocyte progenitors in human cord blood and bone marrow. *J. Exp. Med.* **212**, 385–399 (2015). doi:10.1084/jem.20141442 Medline

9. G. Breton, J. Lee, Y. J. Zhou, J. J. Schreiber, T. Keler, S. Puhr, N. Anandasabapathy, S. Schlesinger, M. Caskey, K. Liu, M. C. Nussenzweig, Circulating precursors of human $CD1c^+$ and $CD141^+$ dendritic cells. *J. Exp. Med.* **212**, 401–413 (2015). doi:10.1084/jem.20141441 Medline

10. M. Cella, D. Jarrossay, F. Facchetti, O. Alebardi, H. Nakajima, A. Lanzavecchia, M. Colonna, Plasmacytoid monocytes migrate to inflamed lymph nodes and produce large amounts of type I interferon. *Nat. Med.* **5**, 919–923 (1999). doi:10.1038/11360 Medline

11. G. Grouard, M.-C. Rissoan, L. Filgueira, I. Durand, J. Banchereau, Y.-J. Liu, The enigmatic plasmacytoid T cells develop into dendritic cells with interleukin (IL)-3 and CD40-ligand. *J. Exp. Med.* **185**, 1101–1112 (1997). doi:10.1084/jem.185.6.1101 Medline

12. S. Doulatov, F. Notta, K. Eppert, L. T. Nguyen, P. S. Ohashi, J. E. Dick, Revised map of the human progenitor hierarchy shows the origin of macrophages and dendritic cells in early lymphoid development. *Nat. Immunol.* **11**, 585–593 (2010). doi:10.1038/ni.1889 Medline

13. J. D. Griffin, K. D. Sabbath, F. Herrmann, P. Larcom, K. Nichols, M. Kornacki, H. Levine, S. A. Cannistra, Differential expression of HLA-DR antigens in subsets of human CFU-GM. *Blood* **66**, 788–795 (1985). Medline

14. A. Dzionek, A. Fuchs, P. Schmidt, S. Cremer, M. Zysk, S. Miltenyi, D. W. Buck, J. Schmitz, BDCA-2, BDCA-3, and BDCA-4: Three markers for distinct subsets of dendritic cells in human peripheral blood. *J. Immunol.* **165**, 6037–6046 (2000). doi:10.4049/jimmunol.165.11.6037 Medline

15. D. A. Jaitin, E. Kenigsberg, H. Keren-Shaul, N. Elefant, F. Paul, I. Zaretsky, A. Mildner, N. Cohen, S. Jung, A. Tanay, I. Amit, Massively parallel single-cell RNA-seq for marker-free decomposition of tissues into cell types. *Science* **343**, 776–779 (2014). doi:10.1126/science.1247651 Medline

16. Sorting strategy from total $Lin^{-}HLA\text{-}DR^{+}CD135^{+}$ cells for MARS-seq.

17. Workflow and quality control of MARS-seq single-cell data analysis.

18. Number of detected genes per cell in the total DC MARS-seq experiment.

19. B. Becher, A. Schlitzer, J. Chen, F. Mair, H. R. Sumatoh, K. W. W. Teng, D. Low, C. Ruedl, P. Riccardi-Castagnoli, M. Poidinger, M. Greter, F. Ginhoux, E. W. Newell, High-dimensional analysis of the murine myeloid cell system. *Nat. Immunol.* **15**, 1181–1189 (2014). doi:10.1038/ni.3006 Medline

20. A. D. Amir, K. L. Davis, M. D. Tadmor, E. F. Simonds, J. H. Levine, S. C. Bendall, D. K. Shenfeld, S. Krishnaswamy, G. P. Nolan, D. Pe'er, viSNE enables visualization of high dimensional single-cell data and reveals phenotypic heterogeneity of leukemia. *Nat. Biotechnol.* **31**, 545–552 (2013). doi:10.1038/nbt.2594 Medline

21. L. Van der Maaten, Visualizing data using t-SNE. *J. Mach. Learn. Res.* **9**, 2579–2625 (2008).

22. M. Ester, H. P. Kriegel, J. Sander, X. Xu, A density-based algorithm for discovering clusters in large spatial databases with noise. *KDD* **1996**, 226–231 (1996).

23. M. Haniffa, A. Shin, V. Bigley, N. McGovern, P. Teo, P. See, P. S. Wasan, X.-N. Wang, F. Malinarich, B. Malleret, A. Larbi, P. Tan, H. Zhao, M. Poidinger, S. Pagan, S. Cookson, R. Dickinson, I. Dimmick, R. F. Jarrett, L. Renia, J. Tam, C. Song, J. Connolly, J. K. Y. Chan, A. Gehring, A. Bertoletti, M. Collin, F. Ginhoux, Human tissues contain CD141hi cross-presenting dendritic cells with functional homology to mouse CD103+ nonlymphoid dendritic cells. *Immunity* **37**, 60–73 (2012). doi:10.1016/j.immuni.2012.04.012 Medline

24. DC subset signature genes derived from Gene Expression Omnibus data series GSE35457 and used for MARS-seq and C1 data analyses.

25. J. Lamb, E. D. Crawford, D. Peck, J. W. Modell, I. C. Blat, M. J. Wrobel, J. Lerner, J. P. Brunet, A. Subramanian, K. N. Ross, M. Reich, H. Hieronymus, G. Wei, S. A. Armstrong, S. J. Haggarty, P. A. Clemons, R. Wei, S. A. Carr, E. S. Lander, T. R. Golub, The Connectivity Map: Using gene-expression signatures to connect small molecules,

genes, and disease. *Science* **313**, 1929–1935 (2006). doi:10.1126/science.1132939 Medline

26. J. Chen, A. Schlitzer, S. Chakarov, F. Ginhoux, M. Poidinger, Mpath maps multi-branching single-cell trajectories revealing progenitor cell progression during development. *Nat. Commun.* **7**, 11988 (2016). doi:10.1038/ncomms11988 Medline

27. C. Trapnell, D. Cacchiarelli, J. Grimsby, P. Pokharel, S. Li, M. Morse, N. J. Lennon, K. J. Livak, T. S. Mikkelsen, J. L. Rinn, The dynamics and regulators of cell fate decisions are revealed by pseudotemporal ordering of single cells. *Nat. Biotechnol.* **32**, 381–386 (2014). doi:10.1038/nbt.2859 Medline

28. M. Setty, M. D. Tadmor, S. Reich-Zeliger, O. Angel, T. M. Salame, P. Kathail, K. Choi, S. Bendall, N. Friedman, D. Pe'er, Wishbone identifies bifurcating developmental trajectories from single-cell data. *Nat. Biotechnol.* **34**, 637–645 (2016). doi:10.1038/nbt.3569 Medline

29. R. R. Coifman, S. Lafon, A. B. Lee, M. Maggioni, B. Nadler, F. Warner, S. W. Zucker, Geometric diffusions as a tool for harmonic analysis and structure definition of data: Multiscale methods. *Proc. Natl. Acad. Sci. U.S.A.* **102**, 7432–7437 (2005). doi:10.1073/pnas.0500896102 Medline

30. J. H. Levine, E. F. Simonds, S. C. Bendall, K. L. Davis, A. D. Amir, M. D. Tadmor, O. Litvin, H. G. Fienberg, A. Jager, E. R. Zunder, R. Finck, A. L. Gedman, I. Radtke, J. R. Downing, D. Pe'er, G. P. Nolan, Data-driven phenotypic dissection of AML reveals progenitor-like cells that correlate with prognosis. *Cell* **162**, 184–197 (2015). doi:10.1016/j.cell.2015.05.047 Medline

31. C. Sadaka, M.-A. Marloie-Provost, V. Soumelis, P. Benaroch, Developmental regulation of MHC II expression and transport in human plasmacytoid-derived dendritic cells. *Blood* **113**, 2127–2135 (2009). doi:10.1182/blood-2008-10-178152 Medline

32. S. L. Jongbloed, A. J. Kassianos, K. J. McDonald, G. J. Clark, X. Ju, C. E. Angel, C.-J. J. Chen, P. R. Dunbar, R. B. Wadley, V. Jeet, A. J. E. Vulink, D. N. J. Hart, K. J. Radford, Human $CD141^+$ $(BDCA\text{-}3)^+$ dendritic cells (DCs) represent a unique myeloid DC subset that cross-presents necrotic cell antigens. *J. Exp. Med.* **207**, 1247–1260 (2010). doi:10.1084/jem.20092140 Medline

33. K. P. A. MacDonald, D. J. Munster, G. J. Clark, A. Dzionek, J. Schmitz, D. N. Hart, Characterization of human blood dendritic cell subsets. *Blood* **100**, 4512–4520 (2002). doi:10.1182/blood-2001-11-0097 Medline

34. T. Matsui, J. E. Connolly, M. Michnevitz, D. Chaussabel, C.-I. Yu, C. Glaser, S. Tindle, M. Pypaert, H. Freitas, B. Piqueras, J. Banchereau, A. K. Palucka, CD2 distinguishes two subsets of human plasmacytoid dendritic cells with distinct phenotype and functions. *J. Immunol.* **182**, 6815–6823 (2009). doi:10.4049/jimmunol.0802008 Medline

35. H. Yu, P. Zhang, X. Yin, Z. Yin, Q. Shi, Y. Cui, G. Liu, S. Wang, P. P. Piccaluga, T. Jiang, L. Zhang, Human $BDCA2^+CD123^+CD56^+$ dendritic cells (DCs) related to blastic plasmacytoid dendritic cell neoplasm represent a unique myeloid DC subset. *Protein Cell* **6**, 297–306 (2015). doi:10.1007/s13238-015-0140-x Medline

36. B. Reizis, A. Bunin, H. S. Ghosh, K. L. Lewis, V. Sisirak, Plasmacytoid dendritic cells: Recent progress and open questions. *Annu. Rev. Immunol.* **29**, 163–183 (2011). doi:10.1146/annurev-immunol-031210-101345 Medline

37. B. Cisse, M. L. Caton, M. Lehner, T. Maeda, S. Scheu, R. Locksley, D. Holmberg, C. Zweier, N. S. den Hollander, S. G. Kant, W. Holter, A. Rauch, Y. Zhuang, B. Reizis, Transcription factor E2-2 is an essential and specific regulator of plasmacytoid dendritic cell development. *Cell* **135**, 37–48 (2008). doi:10.1016/j.cell.2008.09.016 Medline

38. Sorting strategy of $Lin^{-}HLA\text{-}DR^{+}CD33^{+}CD45RA^{+}CD1c^{lo/-}CD2^{+}CADM1^{lo/-}CD123^{+}$ pre-DC for C1 scmRNAseq.

39. Workflow and quality control of C1 scmRNAseq data analysis.

40. Number of expressed genes detected per cell in the pre-DC C1 scmRNAseq experiment.

41. S. C. Bendall, K. L. Davis, A. D. Amir, M. D. Tadmor, E. F. Simonds, T. J. Chen, D. K. Shenfeld, G. P. Nolan, D. Pe'er, Single-cell trajectory detection uncovers progression and regulatory coordination in human B cell development. *Cell* **157**, 714–725 (2014). doi:10.1016/j.cell.2014.04.005 Medline

42. M. Swiecki, M. Colonna, The multifaceted biology of plasmacytoid dendritic cells. *Nat. Rev. Immunol.* **15**, 471–485 (2015). doi:10.1038/nri3865 Medline

43. J. B. Tenenbaum, V. de Silva, J. C. Langford, A global geometric framework for nonlinear dimensionality reduction. *Science* **290**, 2319–2323 (2000). doi:10.1126/science.290.5500.2319 Medline

44. G. E. Grajales-Reyes, A. Iwata, J. Albring, X. Wu, R. Tussiwand, W. Kc, N. M. Kretzer, C. G. Briseño, V. Durai, P. Bagadia, M. Haldar, J. Schönheit, F. Rosenbauer, T. L. Murphy, K. M. Murphy, Batf3 maintains autoactivation of Irf8 for commitment of a $CD8\alpha^{+}$ conventional DC clonogenic progenitor. *Nat. Immunol.* **16**, 708–717 (2015). doi:10.1038/ni.3197 Medline

45. A. Schlitzer, J. Loschko, K. Mair, R. Vogelmann, L. Henkel, H. Einwächter, M. Schiemann, J.-H. Niess, W. Reindl, A. Krug, Identification of $CCR9^{-}$ murine plasmacytoid DC precursors with plasticity to differentiate into conventional DCs. *Blood* **117**, 6562–6570 (2011). doi:10.1182/blood-2010-12-326678 Medline

46. A. Krug, A. Towarowski, S. Britsch, S. Rothenfusser, V. Hornung, R. Bals, T. Giese, H. Engelmann, S. Endres, A. M. Krieg, G. Hartmann, Toll-like receptor expression reveals CpG DNA as a unique microbial stimulus for plasmacytoid dendritic cells which synergizes with CD40 ligand to induce high amounts of IL-12. *Eur. J. Immunol.* **31**, 3026–3037 (2001). doi:10.1002/1521-4141(2001010)31:10<3026:AID-IMMU3026>3.0.CO;2-H Medline

47. A. Dzionek, Y. Inagaki, K. Okawa, J. Nagafune, J. Röck, Y. Sohma, G. Winkels, M. Zysk, Y. Yamaguchi, J. Schmitz, Plasmacytoid dendritic cells: From specific surface markers to specific cellular functions. *Hum. Immunol.* **63**, 1133–1148 (2002). doi:10.1016/S0198-8859(02)00752-8 Medline

48. M. Cella, F. Facchetti, A. Lanzavecchia, M. Colonna, Plasmacytoid dendritic cells activated by influenza virus and CD40L drive a potent TH1 polarization. *Nat. Immunol.* **1**, 305–310 (2000). doi:10.1038/79747 Medline

49. T. Ito, M. Yang, Y.-H. Wang, R. Lande, J. Gregorio, O. A. Perng, X.-F. Qin, Y.-J. Liu, M. Gilliet, Plasmacytoid dendritic cells prime IL-10-producing T regulatory cells by inducible costimulator ligand. *J. Exp. Med.* **204**, 105–115 (2007). doi:10.1084/jem.20061660 Medline

50. J.-F. Fonteneau, M. Gilliet, M. Larsson, I. Dasilva, C. Münz, Y. J. Liu, N. Bhardwaj, Activation of influenza virus-specific $CD4^+$ and $CD8^+$ T cells: A new role for plasmacytoid dendritic cells in adaptive immunity. *Blood* **101**, 3520–3526 (2003). doi:10.1182/blood-2002-10-3063 Medline

51. G. Hoeffel, A.-C. Ripoche, D. Matheoud, M. Nascimbeni, N. Escriou, P. Lebon, F. Heshmati, J.-G. Guillet, M. Gannagé, S. Caillat-Zucman, N. Casartelli, O. Schwartz, H. De la Salle, D. Hanau, A. Hosmalin, C. Marañón, Antigen crosspresentation by human plasmacytoid dendritic cells. *Immunity* **27**, 481–492 (2007). doi:10.1016/j.immuni.2007.07.021 Medline

52. Y.-J. Liu, IPC: Professional type 1 interferon-producing cells and plasmacytoid dendritic cell precursors. *Annu. Rev. Immunol.* **23**, 275–306 (2005). doi:10.1146/annurev.immunol.23.021704.115633 Medline

53. F. P. Siegal, N. Kadowaki, M. Shodell, P. A. Fitzgerald-Bocarsly, K. Shah, S. Ho, S. Antonenko, Y. J. Liu, The nature of the principal type 1 interferon-producing cells in human blood. *Science* **284**, 1835–1837 (1999). doi:10.1126/science.284.5421.1835 Medline

54. C. F. de Winter, M. Baas, E. K. Bijlsma, J. van Heukelingen, S. Routledge, R. C. M. Hennekam, Phenotype and natural history in 101 individuals with Pitt-Hopkins syndrome through an internet questionnaire system. *Orphanet J. Rare Dis.* **11**, 37 (2016). doi:10.1186/s13023-016-0422-2 Medline

55. B. Langmead, C. Trapnell, M. Pop, S. L. Salzberg, Ultrafast and memory-efficient alignment of short DNA sequences to the human genome. *Genome Biol.* **10**, R25 (2009). doi:10.1186/gb-2009-10-3-r25 Medline

56. A. Yates, W. Akanni, M. R. Amode, D. Barrell, K. Billis, D. Carvalho-Silva, C. Cummins, P. Clapham, S. Fitzgerald, L. Gil, C. G. Girón, L. Gordon, T. Hourlier, S. E. Hunt, S. H. Janacek, N. Johnson, T. Juettemann, S. Keenan, I. Lavidas, F. J. Martin, T. Maurel, W. McLaren, D. N. Murphy, R. Nag, M. Nuhn, A. Parker, M. Patricio, M. Pignatelli, M. Rahtz, H. S. Riat, D. Sheppard, K. Taylor, A. Thormann, A. Vullo, S. P. Wilder, A. Zadissa, E. Birney, J. Harrow, M. Muffato, E. Perry, M. Ruffier, G. Spudich, S. J. Trevanion, F. Cunningham, B. L. Aken, D. R. Zerbino, P. Flicek, Ensembl 2016. *Nucleic Acids Res.* **44**, D710–D716 (2016). doi:10.1093/nar/gkv1157 Medline

57. D. Grün, A. Lyubimova, L. Kester, K. Wiebrands, O. Basak, N. Sasaki, H. Clevers, A. van Oudenaarden, Single-cell messenger RNA sequencing reveals rare intestinal cell types. *Nature* **525**, 251–255 (2015). doi:10.1038/nature14966 Medline

58. R. Satija, J. A. Farrell, D. Gennert, A. F. Schier, A. Regev, Spatial reconstruction of single-cell gene expression data. *Nat. Biotechnol.* **33**, 495–502 (2015). doi:10.1038/nbt.3192 Medline

59. M. Hahsler, M. Piekenbrock, dbscan: Density Based Clustering of Applications with Noise (DBSCAN) and Related Algorithms. R package version 1.0-0; https://CRAN.R-project.org/package=dbscan (2017).

60. J. Harrow, A. Frankish, J. M. Gonzalez, E. Tapanari, M. Diekhans, F. Kokocinski, B. L. Aken, D. Barrell, A. Zadissa, S. Searle, I. Barnes, A. Bignell, V. Boychenko, T. Hunt, M. Kay, G. Mukherjee, J. Rajan, G. Despacio-Reyes, G. Saunders, C. Steward, R. Harte, M. Lin, C. Howald, A. Tanzer, T. Derrien, J. Chrast, N. Walters, S. Balasubramanian, B. Pei, M. Tress, J. M. Rodriguez, I. Ezkurdia, J. van Baren, M. Brent, D. Haussler, M. Kellis, A. Valencia, A. Reymond, M. Gerstein, R. Guigó, T. J. Hubbard, GENCODE: The reference human genome annotation for The ENCODE Project. *Genome Res.* **22**, 1760–1774 (2012). doi:10.1101/gr.135350.111 Medline

61. B. Li, C. N. Dewey, RSEM: Accurate transcript quantification from RNA-seq data with or without a reference genome. *BMC Bioinformatics* **12**, 323 (2011). doi:10.1186/1471-2105-12-323 Medline

62. R. Finck, E. F. Simonds, A. Jager, S. Krishnaswamy, K. Sachs, W. Fantl, D. Pe'er, G. P. Nolan, S. C. Bendall, Normalization of mass cytometry data with bead standards. *Cytometry A* **83A**, 483–494 (2013). doi:10.1002/cyto.a.22271 Medline

63. E. W. Newell, N. Sigal, S. C. Bendall, G. P. Nolan, M. M. Davis, Cytometry by time-of-flight shows combinatorial cytokine expression and virus-specific cell niches within a continuum of $CD8^+$ T cell phenotypes. *Immunity* **36**, 142–152 (2012). doi:10.1016/j.immuni.2012.01.002 Medline

64. D. R. Parks, M. Roederer, W. A. Moore, A new "Logicle" display method avoids deceptive effects of logarithmic scaling for low signals and compensated data. *Cytometry A* **69A**, 541–551 (2006). doi:10.1002/cyto.a.20258 Medline

65. J. Oksanen *et al*., vegan: Community Ecology Package. R package version 2.4-2. https://CRAN.R-project.org/package=vegan (2017).

66. H. Chen, M. C. Lau, M. T. Wong, E. W. Newell, M. Poidinger, J. Chen, Cytofkit: A bioconductor package for an integrated mass cytometry data analysis pipeline. *PLOS Comput. Biol.* **12**, e1005112 (2016). doi:10.1371/journal.pcbi.1005112 Medline

67. G. K. Smyth, Linear models and empirical Bayes methods for assessing differential expression in microarray experiments. *Stat. Appl. Genet. Mol. Biol.* **3**, 1–25(2004). doi:10.2202/1544-6115.1027 Medline

68. Y. Benjamini, Y. Hochberg, Controlling the false discovery rate: A practical and powerful approach to multiple testing. *J. R. Stat. Soc. B* **57**, 289–300 (1995).

69. Lists of genes identified from the microarray DEG analysis comparisons along the lineage progression from early pre-DC to mature cDC, for cDC1 and cDC2 respectively, and the list of the 62 common genes.

70. Venn diagram comparison of the two lists of DEGs and identification of the 62 common genes.

71. E. Mass, I. Ballesteros, M. Farlik, F. Halbritter, P. Günther, L. Crozet, C. E. Jacome-Galarza, K. Händler, J. Klughammer, Y. Kobayashi, E. Gomez-Perdiguero, J. L. Schultze, M.

Beyer, C. Bock, F. Geissmann, Specification of tissue-resident macrophages during organogenesis. *Science* **353**, aaf4238 (2016). doi:10.1126/science.aaf4238 Medline

72. G. X. Y. Zheng, J. M. Terry, P. Belgrader, P. Ryvkin, Z. W. Bent, R. Wilson, S. B. Ziraldo, T. D. Wheeler, G. P. McDermott, J. Zhu, M. T. Gregory, J. Shuga, L. Montesclaros, J. G. Underwood, D. A. Masquelier, S. Y. Nishimura, M. Schnall-Levin, P. W. Wyatt, C. M. Hindson, R. Bharadwaj, A. Wong, K. D. Ness, L. W. Beppu, H. J. Deeg, C. McFarland, K. R. Loeb, W. J. Valente, N. G. Ericson, E. A. Stevens, J. P. Radich, T. S. Mikkelsen, B. J. Hindson, J. H. Bielas, Massively parallel digital transcriptional profiling of single cells. *Nat. Commun.* **8**, 14049 (2017). doi:10.1038/ncomms14049 Medline

73. F. Paul, Y. Arkin, A. Giladi, D. A. Jaitin, E. Kenigsberg, H. Keren-Shaul, D. Winter, D. Lara-Astiaso, M. Gury, A. Weiner, E. David, N. Cohen, F. K. B. Lauridsen, S. Haas, A. Schlitzer, A. Mildner, F. Ginhoux, S. Jung, A. Trumpp, B. T. Porse, A. Tanay, I. Amit, Transcriptional heterogeneity and lineage commitment in myeloid progenitors. *Cell* **163**, 1663–1677 (2015). doi:10.1016/j.cell.2015.11.013 Medline

74. O. Matcovitch-Natan, D. R. Winter, A. Giladi, S. Vargas Aguilar, A. Spinrad, S. Sarrazin, H. Ben-Yehuda, E. David, F. Zelada González, P. Perrin, H. Keren-Shaul, M. Gury, D. Lara-Astaiso, C. A. Thaiss, M. Cohen, K. Bahar Halpern, K. Baruch, A. Deczkowska, E. Lorenzo-Vivas, S. Itzkovitz, E. Elinav, M. H. Sieweke, M. Schwartz, I. Amit, Microglia development follows a stepwise program to regulate brain homeostasis. *Science* **353**, aad8670 (2016). doi:10.1126/science.aad8670 Medline

75. J. A. Donovan, G. A. Koretzky, CD45 and the immune response. *J. Am. Soc. Nephrol.* **4**, 976–985 (1993). Medline

76. L. Ziegler-Heitbrock, P. Ancuta, S. Crowe, M. Dalod, V. Grau, D. N. Hart, P. J. M. Leenen, Y.-J. Liu, G. MacPherson, G. J. Randolph, J. Scherberich, J. Schmitz, K. Shortman, S. Sozzani, H. Strobl, M. Zembala, J. M. Austyn, M. B. Lutz, Nomenclature of monocytes and dendritic cells in blood. *Blood* **116**, e74–e80 (2010). doi:10.1182/blood-2010-02-258558 Medline

77. F. Nakayama, S. Nishihara, H. Iwasaki, T. Kudo, R. Okubo, M. Kaneko, M. Nakamura, M. Karube, K. Sasaki, H. Narimatsu, CD15 expression in mature granulocytes is determined by alpha 1,3-fucosyltransferase IX, but in promyelocytes and monocytes by alpha 1,3-fucosyltransferase IV. *J. Biol. Chem.* **276**, 16100–16106 (2001). doi:10.1074/jbc.M007272200 Medline

78. J. M. Milush, B. R. Long, J. E. Snyder-Cappione, A. J. Cappione 3rd, V. A. York, L. C. Ndhlovu, L. L. Lanier, J. Michaëlsson, D. F. Nixon, Functionally distinct subsets of human NK cells and monocyte/DC-like cells identified by coexpression of CD56, CD7, and CD4. *Blood* **114**, 4823–4831 (2009). doi:10.1182/blood-2009-04-216374 Medline

79. F. Schütz, H. Hackstein, Identification of novel dendritic cell subset markers in human blood. *Biochem. Biophys. Res. Commun.* **443**, 453–457 (2014). doi:10.1016/j.bbrc.2013.11.112 Medline

80. B. Morandi, R. Costa, M. Falco, S. Parolini, A. De Maria, G. Ratto, M. C. Mingari, G. Melioli, A. Moretta, G. Ferlazzo, Distinctive lack of CD48 expression in subsets of human dendritic cells tunes NK cell activation. *J. Immunol.* **175**, 3690–3697 (2005). doi:10.4049/jimmunol.175.6.3690 Medline

81. H. Strobl, C. Scheinecker, E. Riedl, B. Csmarits, C. Bello-Fernandez, W. F. Pickl, O. Majdic, W. Knapp, Identification of $CD68^{+}lin^{-}$ peripheral blood cells with dendritic precursor characteristics. *J. Immunol.* **161**, 740–748 (1998). Medline

82. L. Galibert, G. S. Diemer, Z. Liu, R. S. Johnson, J. L. Smith, T. Walzer, M. R. Comeau, C. T. Rauch, M. F. Wolfson, R. A. Sorensen, A.-R. Van der Vuurst de Vries, D. G. Branstetter, R. M. Koelling, J. Scholler, W. C. Fanslow, P. R. Baum, J. M. Derry, W. Yan, Nectin-like protein 2 defines a subset of T-cell zone dendritic cells and is a ligand for class-I-restricted T-cell-associated molecule. *J. Biol. Chem.* **280**, 21955–21964 (2005). doi:10.1074/jbc.M502095200 Medline

83. M. Cheng, X. Zhang, H. Yu, P. Du, J. Plumas, L. Chaperot, L. Su, L. Zhang, Characterization of species-specific genes regulated by E2-2 in human plasmacytoid dendritic cells. *Sci. Rep.* **5**, 10752 (2015). doi:10.1038/srep10752 Medline

84. M. Haniffa, V. Bigley, M. Collin, Human mononuclear phagocyte system reunited. *Semin. Cell Dev. Biol.* **41**, 59–69 (2015). doi:10.1016/j.semcdb.2015.05.004 Medline

85. L. F. Poulin, M. Salio, E. Griessinger, F. Anjos-Afonso, L. Craciun, J.-L. Chen, A. M. Keller, O. Joffre, S. Zelenay, E. Nye, A. Le Moine, F. Faure, V. Donckier, D. Sancho, V. Cerundolo, D. Bonnet, C. Reis e Sousa, Characterization of human DNGR-1+ BDCA3+ leukocytes as putative equivalents of mouse CD8alpha+ dendritic cells. *J. Exp. Med.* **207**, 1261–1271 (2010). doi:10.1084/jem.20092618 Medline

86. P. B. Watchmaker, K. Lahl, M. Lee, D. Baumjohann, J. Morton, S. J. Kim, R. Zeng, A. Dent, K. M. Ansel, B. Diamond, H. Hadeiba, E. C. Butcher, Comparative transcriptional and functional profiling defines conserved programs of intestinal DC differentiation in humans and mice. *Nat. Immunol.* **15**, 98–108 (2014). doi:10.1038/ni.2768 Medline

87. C. Weber, K. U. Belge, P. von Hundelshausen, G. Draude, B. Steppich, M. Mack, M. Frankenberger, K. S. Weber, H. W. Ziegler-Heitbrock, Differential chemokine receptor expression and function in human monocyte subpopulations. *J. Leukoc. Biol.* **67**, 699–704 (2000). Medline

88. U. O'Doherty, M. Peng, S. Gezelter, W. J. Swiggard, M. Betjes, N. Bhardwaj, R. M. Steinman, Human blood contains two subsets of dendritic cells, one immunologically mature and the other immature. *Immunology* **82**, 487–493 (1994). Medline